iScience

CellPress
OPEN ACCESS

Article

Myeloid-intrinsic cell cycle-related kinase drives immunosuppression to promote tumorigenesis

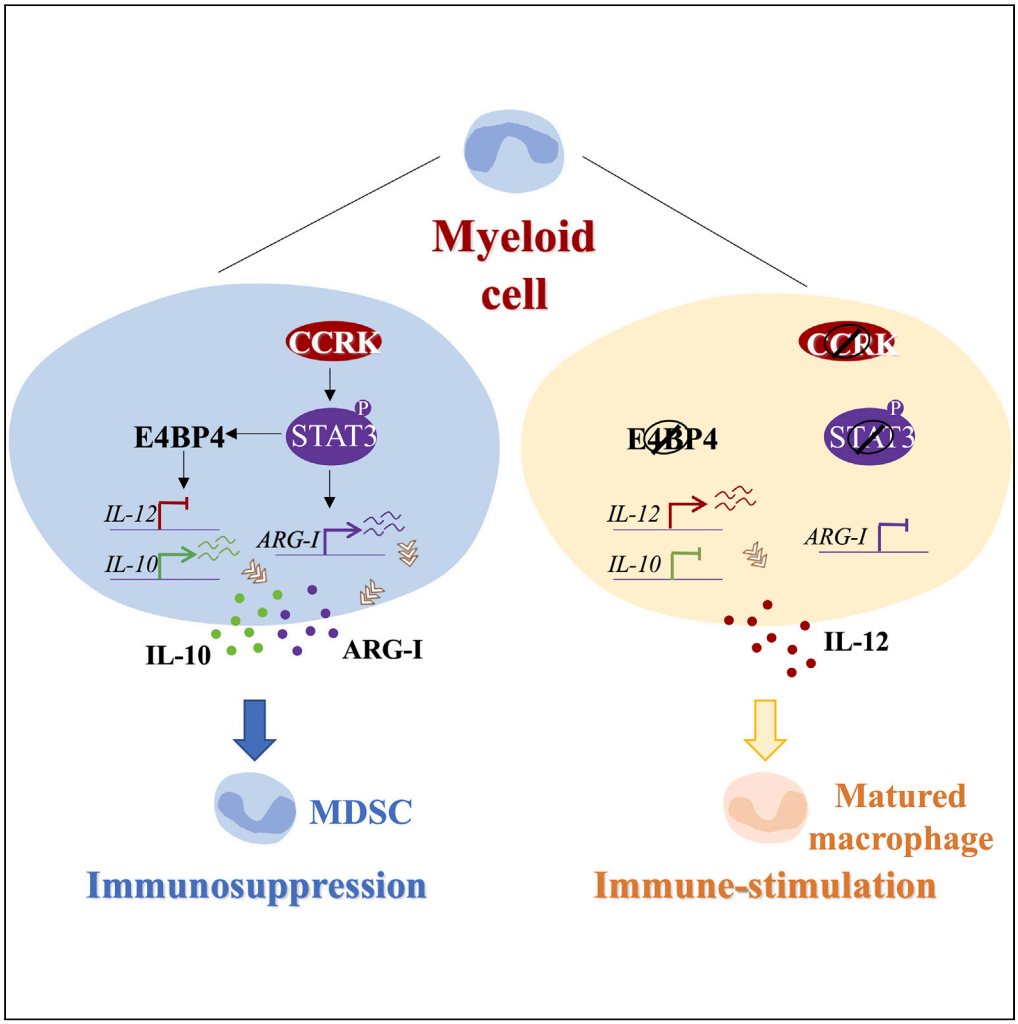

Jingying Zhou, Huanyu Wang, Ting Shu, ..., King-Lau Chow, Joseph Jao-yiu Sung, Alfred Sze-Lok Cheng

alfredcheng@cuhk.edu.hk

Highlights

Myeloid CCRK expression is elevated in mice and human with hepatocellular carcinoma

Inactivation of myeloid CCRK limits HCC progression and prolongs survival

CCRK maintains the immature status and immunosuppressive capacity of MDSCs

CCRK induces STAT3 phosphorylation to control E4BP4 transcriptional activity in MDSCs

Zhou et al., iScience 26, 107626
October 20, 2023
https://doi.org/10.1016/j.isci.2023.107626

iScience

CellPress
OPEN ACCESS

Article

Myeloid-intrinsic cell cycle-related kinase drives immunosuppression to promote tumorigenesis

Jingying Zhou,[1,9] Huanyu Wang,[1,9] Ting Shu,[1] Jing Wang,[1] Weiqin Yang,[1] Jingqing Li,[1] Lipeng Ding,[1] Man Liu,[2] Hanyong Sun,[3] John Wong,[4] Paul Bo-san Lai,[4] Shun-Wa Tsang,[5] Simon E. Ward,[6] King-Lau Chow,[5] Joseph Jao-yiu Sung,[7,8] and Alfred Sze-Lok Cheng[1,10,*]

SUMMARY

Massive expansion of immature and suppressive myeloid cells is a common feature of malignant solid tumors. Over-expression of cyclin-dependent kinase 20, also known as cell cycle-related kinase (CCRK), in hepatocellular carcinoma (HCC) correlates with reduced patient survival and low immunotherapy responsiveness. Beyond tumor-intrinsic oncogenicity, here we demonstrated that CCRK is upregulated in myeloid cells in tumor-bearing mice and in patients with HCC. Intratumoral injection of *Ccrk*-knockdown myeloid-derived suppressor cells (MDSCs) increased tumor-infiltrating $CD8^+$T cells and suppressed HCC tumorigenicity. Using an indel mutant transgenic model, we showed that *Ccrk* inactivation in myeloid cells conferred a mature phenotype with elevated IL-12 production, driving Th1 responses and $CD8^+$T cell cytotoxicity to reduce orthotopic tumor growth and prolong survival. Mechanistically, CCRK activates STAT3/E4BP4 signaling in MDSCs to acquire immunosuppressive activity through transcriptional IL-10 induction and IL-12 suppression. Taken together, our findings unravel mechanistic insights into MDSC-mediated immunosuppression and offer a therapeutic kinase-target for cancer immunotherapy.

INTRODUCTION

The critical role of myeloid cells in regulating anti-tumor immune responses and tumor progression is well established.[1] Substantial expansion of immature and immunosuppressive myeloid cells like myeloid-derived suppressor cells (MDSCs) is one of the common and important clinically relevant features of various cancers.[1,2] Taking hepatocellular carcinoma (HCC) as an example, accumulating evidence has demonstrated that MDSC accumulation, both $CD15^+$ polymorphonuclear (PMN) and $CD14^+$ monocytic (M)-MDSC subtypes in peripheral blood or tumor tissues, associates with poor prognosis and immunotherapy resistance in patients.[3–5] Therapies that target MDSC to relieve immune suppression therefore represent promising strategies to better control HCC.

There are various ongoing preclinical and clinical studies on developing MDSC-targeting therapies, including targeting tumor-secreted growth factors, counteracting the suppressive activity of MDSCs, or driving differentiation of these immature myeloid cells into antigen presentation cells (APCs), which are crucial for T cell priming and activation.[1] For example, celecoxib, which can block the immunosuppressive arginase-I (ARG-I) expression in MDSC, was shown to reduce tumor progression in AB1 mesothelioma and 3LL lung carcinoma mouse models.[6,7] In addition, drugs that induce MDSC differentiation into mature APCs, like all-trans-retinoic acid (ATRA), an FDA-approved standard-of-care treatment for acute promyelocytic leukemia (APL), could induce macrophage and dendritic cell (DC) differentiation via binding to RA receptor alpha (RAR) and triggering downstream transcriptional reprogramming.[8] Moreover, similar differentiation effects could be observed by chemotherapeutic agent treatment on *in vitro*-generated MDSCs.[9] However, most evidence of therapeutic targeting of MDSCs in human comes from secondary observations in patients undergoing standard or experimental therapies.[10] Therefore, understanding the transcriptional regulatory mechanisms of MDSC identity will be essential to develop methods for specific therapeutic targeting.

One of the major transcriptional regulatory factors that drive MDSC expansion and immunosuppressive function in cancer is signal-transducer-and-activator-of-transcription 3 (STAT3).[1,11,12] STAT3 is critically important for cell proliferation, survival, and motility, which is activated by phosphorylation at Tyr 705 or Ser 727.[10] Ablation of STAT3 expression, using conditional knockout mice or selective STAT3 inhibitors, is

[1]School of Biomedical Sciences, The Chinese University of Hong Kong, Hong Kong SAR 999077, China
[2]Department of Gastroenterology, The First Affiliated Hospital, Sun Yat-sen University, Guangzhou, China
[3]Department of Liver Surgery, Ren Ji Hospital, School of Medicine, Shanghai Jiao Tong University, Shanghai, China
[4]Department of Surgery, The Chinese University of Hong Kong, Hong Kong SAR 999077, China
[5]Division of Life Science, Hong Kong University of Science and Technology, Hong Kong SAR 999077, China
[6]Medicines Discovery Institute, Cardiff University, Main Building, Park Place, Cardiff CF10 3AT, UK
[7]Lee Kong Chian School of Medicine, Nanyang Technological University, Singapore, Singapore
[8]State Key Laboratory of Digestive Disease, The Chinese University of Hong Kong, Hong Kong SAR 999077, China
[9]These authors contributed equally
[10]Lead contact
*Correspondence: alfredcheng@cuhk.edu.hk
https://doi.org/10.1016/j.isci.2023.107626

reported to markedly reduce the expansion of MDSC and increased T cell responses in tumor-bearing mice.[10] Mechanistically, STAT3 can upregulate *ARG-I* transcription by binding to its promoter region in MDSCs isolated from tumor-bearing mice as well as cancer patients.[11] In addition, activation of myeloid STAT3 prevents the differentiation of immature myeloid cells into mature DCs and macrophages systemically or in the tumor microenvironment (TME).[13,14] Furthermore, a phase Ib trial (NCT01563302) revealed that systemic administration of AZD9150, an antisense oligonucleotide inhibitor of STAT3, reduced the levels of peripheral PMN-MDSCs in patients with diffuse large B cell lymphoma (DLBCL),[15] and is now in a phase II clinical trial in combination with immune checkpoint inhibitors (ICIs) in patients with advanced solid tumors and metastatic squamous cell carcinoma of the head and neck (NCT02499328). However, MDSC targeting via abolishing STAT3 signaling was also reported to cause side effects like hyper-IgE syndrome in some patients, which is likely related to the physiological function of STAT3 in other cell types.[16]

Cyclin-dependent kinases (CDKs), fundamental drivers of cell cycle and function in various DNA damage responses, have long been regarded as promising therapeutic targets in cancer.[17] Further studies also pinpointed the essential roles of CDKs in the transcriptional control of immune cells.[18] For example, CDK2 and CDK4/6 are highly expressed in T cells, which are associated with the activation of Treg and suppression of memory $CD8^+$T cell formation, respectively.[19–21] In addition, CDK7 and CDK9 could specifically regulate neutrophil transcription and survival.[22] We have uncovered that the latest CDK family member, CDK20 or cell cycle-related kinase (CCRK), is a signaling hub that is overexpressed in hepatoma cells and functions in promoting HCC development and liver metastasis.[4,23–25] Deletion of hepatoma *Ccrk* suppresses tumor-intrinsic oncogenic pathway and reduces HCC proliferation, and disrupts the cross-talk between tumor and MDSCs in TME, which in turn lead to tumor suppression and better therapeutic efficacy of anti-programmed death 1 (PD1)/PD1-ligand 1 (PD-L1) antibody *in vivo*.[4,25,26] Here, we further identified a tumor-induced CCRK upregulation in myeloid cells as a key player for cancer immune escape. Inhibition of myeloid CCRK could therefore overcome tumor immunosuppression and re-invigorate adaptive anti-tumor immunity to control HCC progression.

RESULT

CCRK is selectively upregulated in myeloid cells from tumor-bearing mice and patients with HCC

To explore the expression pattern of CCRK in immune cells, we isolated $CD45^+$leukocytes and sorted the $CD19^+$B cells, $CD3^+$T cells, $NK1.1^+$ natural killer (NK) cells, and $CD11b^+$myeloid cells from the spleen of naive C57BL/6 mice, or the spleen and tumor of C57BL/6 mice subcutaneously inoculated with a hepatoma RIL-175 cell line (Figure 1A).[27] Of note, no CCRK expression was observed in all the major immune cells from naive mouse splenocytes (Figure 1A). In comparison, a selective upregulation of CCRK expression in myeloid cells from both splenocytes and tumor-infiltrating leukocytes (TILs) was detected in tumor-bearing mice (Figure 1A), suggesting a potential effect of tumor-derived factors in CCRK upregulation. When we further sorted myeloid cells into $CD11b^+Gr\text{-}1^+$MDSCs and $CD11b^+Gr\text{-}1^-$ones which contained $CD11c^+$DCs and $F4/80^+$macrophages, we found that CCRK showed significantly higher expressions in $CD11b^+Gr\text{-}1^+$MDSCs from both splenocytes and TILs (Figure 1B). To determine whether CCRK upregulation in myeloid cells from tumor-bearing host is translatable into the human context, $CD11b^+CD33^+$myeloid cells were then sorted from peripheral blood mononuclear cells (PBMCs), liver and tumor tissues of patients with HCC. $CD11b^+CD33^+$myeloid cells sorted from healthy donor (HD) PBMCs were served as control. By quantitative RT-PCR (qRT-PCR), we observed a consistent upregulation of *CCRK* mRNA expression in myeloid cells from patients with HCC compared to HD controls ($p < 0.05$; Figure 1C). Taken together, we found that CCRK is selectively upregulated in myeloid cells from tumor-bearing hosts. Since massive expansion of tumor-associated myeloid cells contributes to tumor immune escape and progression, we next explored the functional significance of this aberrant myeloid CCRK upregulation *in vivo*.

Ccrk expression maintains the immature status of MDSCs to support tumor growth *in vivo*

To explore the functional significance of *Ccrk* expression in myeloid cell-mediated immunosuppression and tumor growth, a myeloid cell-competent lentivirus backbone that packed with GFP-expressing short hairpin RNA (shRNA) was introduced.[28] Since CCRK expression was significantly higher in $CD11b^+Gr\text{-}1^+$MDSCs in tumor-bearing mice (Figure 1B), we adopted an *in vitro* protocol to generate MDSCs from bone marrows (BMs) by mouse recombinant IL-6 and granulocyte-macrophage colony-stimulating factor (GM-CSF). Red-fluorescence protein $(RFP)^{+/+}$ transgenic mice were used as BM source for *in vivo* cell tracking[4] (Figure 2A). Compared to naive immature myeloid cells (IMCs), we first confirmed that BM-MDSCs showed remarkable upregulation of CCRK, as well as of typical MDSC markers p-$STAT3^{Tyr705}$ and ARG-I (Figures S1A and S1B). We then used the myeloid cell-competent lentivirus packed with shRNA against *Ccrk*[26] (LV-sh*Ccrk*) to knockdown *Ccrk* expressions in these RFP^+BM-MDSCs (Figure 2A). Interestingly, compared to sh*Ctrl* control (LV-sh*Ctrl*), LV-sh*Ccrk* not only successfully reduced CCRK expression, but also significantly downregulated p-$STAT3^{Tyr705}$ and ARG-I in BM-MDSCs (Figure 2A). These data suggested that CCRK might regulate the STAT3 pathway and control MDSC immunosuppression. Thus, we further sorted these lentivirus-sh*Ctrl* or -sh*Ccrk* infected GFP^+RFP^+MDSCs by fluorescence-activated cell sorting (FACS) and then intratumorally injected into the left or right subcutaneous tumors of the same recipient C57BL/6 mouse at day 6 post tumor inoculation (Figure 3A). Of note, the subcutaneous tumor growth rate as well as endpoint tumor weight were significantly reduced in MDSC-sh*Ccrk*-injected tumors compared to those injected with MDSC-sh*Ctrl* ($p < 0.05$; Figures 2B and 2C), accompanied with increased $CD8^+$T cell numbers ($p < 0.05$; Figure 2D). To further study how does CCRK regulate MDSC immature status, we analyzed the myeloid cell proportions in the RFP^+ cells at 24 h post adoptive transfer in naive C57BL/6 mice (Figure 2A). Interestingly, we observed an alteration of RFP^+ adoptive transferred cell components from MDSC-sh*Ccrk* injected mice, with decreased percentages of $CD11b^+Gr\text{-}1^+Ly6G^+Ly6C^{int}$PMN-MDSCs, but increased proportions of $F4/80^+CD11c^-$ macrophages when compared to MDSC-sh*Ctrl* injected mice ($p < 0.05$; Figures 2E and 2F). In parallel, these $F4/80^+CD11c^-$ cells also displayed upregulated CD86 and CD80 when *Ccrk* was knocked down ($p < 0.05$; Figure 2G), suggesting that knockdown of *Ccrk* might induce MDSC differentiation

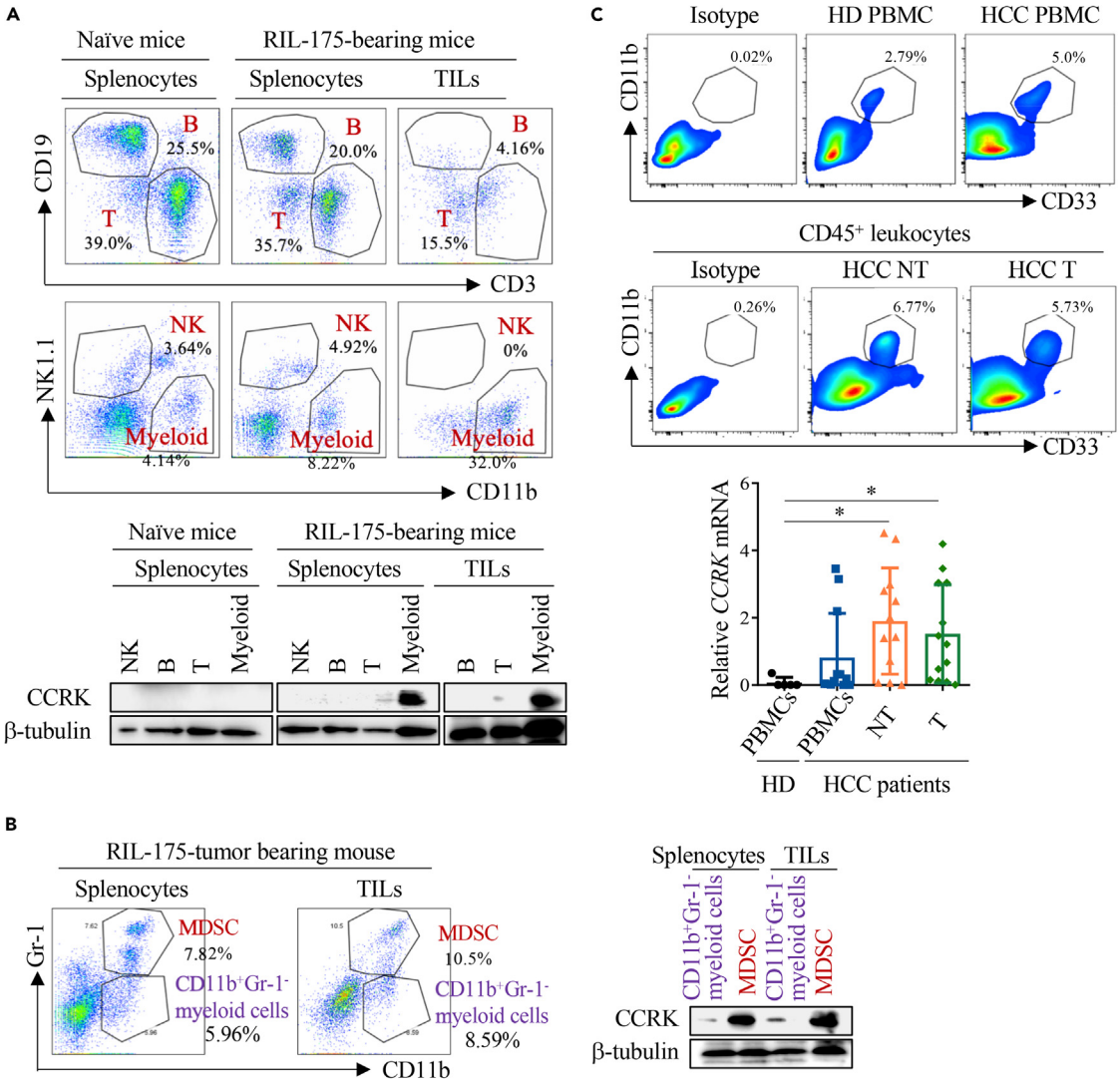

Figure 1. CCRK is upregulated and selectively expressed in myeloid cells from tumor-bearing mice and patients with HCC

(A) Representative flow cytometry dot plots of $CD19^+$B cells, $CD3^+$T cells, $CD11b^+$ myeloid cells, and $NK1.1^+$NK cells in splenocytes of naive mice, splenocytes and tumor infiltrating leukocytes (TILs) of RIL-175 tumor-bearing mice. These cells were sorted by FACS and used to detect CCRK expression by western blot. ($n \geq 3$).

(B) Representative flow cytometry dot plots of $CD11b^+Gr\text{-}1^+$MDSCs and $CD11b^+Gr\text{-}1^-$myeloid cells from splenocytes and TILs of RIL-175 tumor-bearing mice. CCRK expression was measured by western blot. β-tubulin was served as loading control. Representative data from at least three independent experiments are shown. ($n \geq 3$).

(C) $CD11b^+CD33^+$myeloid cells sorted from the peripheral blood mononuclear cells (PBMCs) of healthy donors (HD), PBMCs, adjacent non-tumor (NT), and tumor (T) tissues of HCC patients for the measurement of *CCRK* mRNA expression (relative to *GAPDH*) by qRT-PCR. ($n \geq 5$). *$p < 0.05$.

into mature macrophage-like cells. Next, we generated a *Ccrk* knockdown RIL-175 stable line to exclude the possible effect of tumoral CCRK expression in this setting (Figure S2A). Although the growth rate of RIL-sh*Ccrk* tumors was impaired compared to wild-type (WT) RIL-175, MDSC-sh*Ccrk*-injected tumors consistently showed slower tumor growth rate as well as decreased endpoint tumor weights compared to those injected with MDSC-sh*Ctrl* (Figures S2B and S2C). Taken together, our findings demonstrated that CCRK maintained the immature status and tumor supportive functions of MDSCs, independent of tumoral CCRK expression *in vivo*.

Inactivation of myeloid *Ccrk* leads to the remodeling of immunosuppressive TME and tumor suppression in *Ccrk*$^{indel/indel}$ transgenic mouse model

To further confirm the roles of myeloid *Ccrk* in orthotopic tumor progression, we constructed a host *Ccrk* inactivated transgenic (TG) mouse strain (Figure 3A). As an essential kinase needed for embryonic development, knockout of the whole *Ccrk* gene resulted in miscarriage.[29] Therefore, we adopted the CRISPR/Cas9 platform by injecting the CRISPR-Cas9 mRNA and *Ccrk* sgRNA into the zygotes of WT C57BL/6

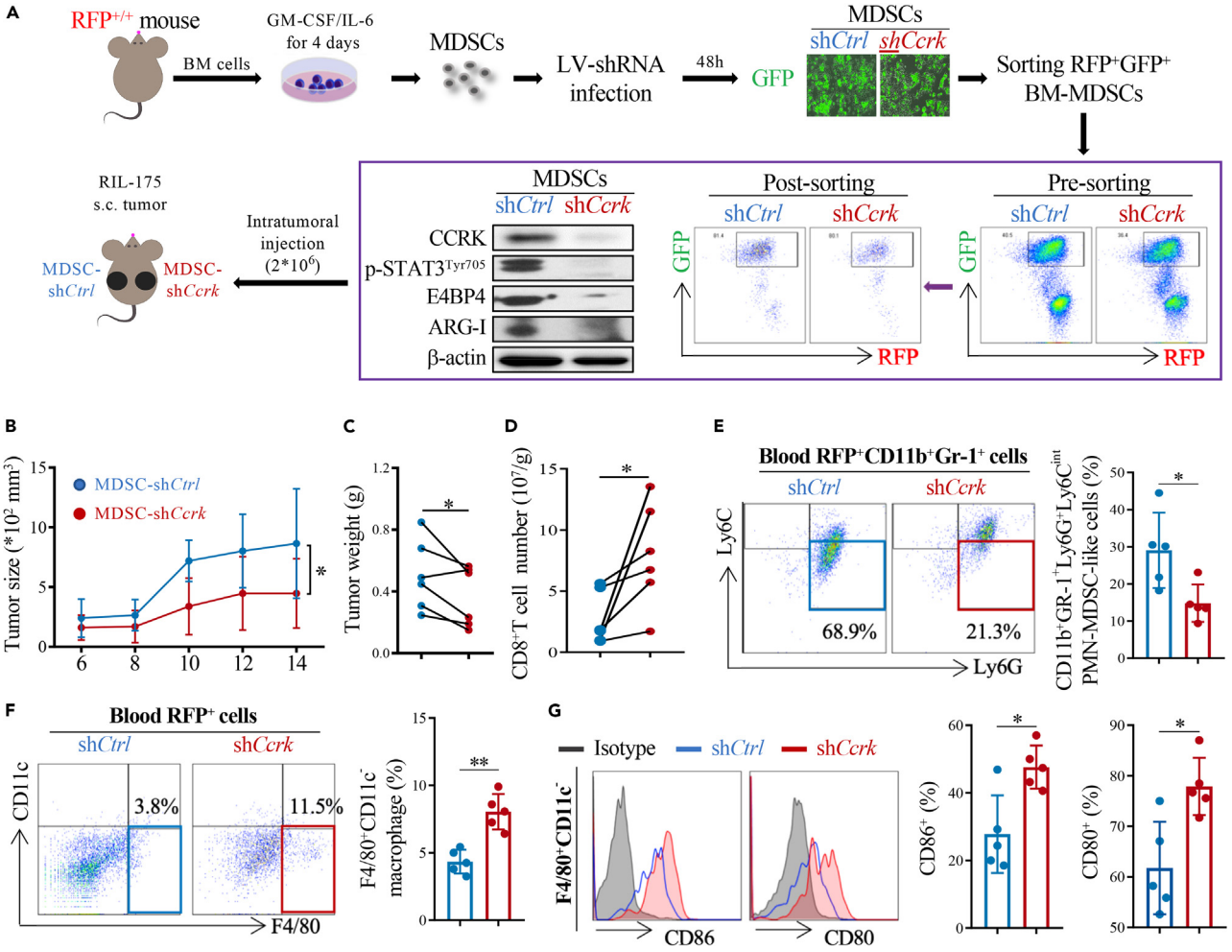

Figure 2. *Ccrk* expression maintains the immature status of MDSCs to support tumor growth *in vivo*

(A) Schematic diagram. MDSCs were generated from naive RFP$^{+/+}$mouse bone marrows (BMs), treated with IL-6/GM-CSF for four days, and infected with lentivirus (LV)-based sh*Ctrl*-GFP or sh*Ccrk*-GFP (1 MOI) for 48 h. The success of virus infection, sorting purifies and expressions of CCRK, p-STAT3^{Tyr705}, E4BP4, and ARG-I were confirmed by fluorescent-microscope or western blot, respectively, in FACS sorted RFP^{+}GFP^{+}MDSCs at 48-h post infection. β-actin was served as loading control. 2*10^{6} purified MDSCs were then intratumorally injected into the left or right subcutaneous tumors of the same RIL-175-bearing mouse at day 6 post tumor inoculation for tumor growth analysis.

(B) Tumor sizes were measured by caliper every two days and expressed as ½*(length*width^{2}).

(C and D) (C) Tumor weights, and (D) the absolute numbers of tumor-infiltrating CD8^{+}T cells were measured at the endpoint (n = 6).

(E and F) (E) Blood was collected at 24-h post 2*10^{6} RFP^{+}GFP^{+}MDSCs adoptive transfer in naive C57BL/6 mice for MDSC phenotype analysis *in vivo*. The representative flow cytometry dot plots and proportions of CD11b^{+}Gr-1^{+}Ly6G^{+}Ly6C^{int}PMN-MDSCs as well as (F) F4/80^{+}CD11c^{-}macrophages in RFP^{+} adoptive transferred cells are shown.

(G) The expressions of CD86 and CD80 on F4/80^{+}CD11c^{-}macrophages are shown in overlay histograms and bar charts. (n = 5). Data are presented as mean ± SD. *p < 0.05. **p < 0.01.

See also Figures S1 and S2.

mouse, aiming at inducing nucleotide deletion or insertion in exons 1 and 3 of *Ccrk* locus, respectively. We then successfully generated a TG mouse strain carrying a homozygous *Ccrk* indel mutant (*Ccrk*$^{indel/indel}$) with an insertion of ATC (encode amino acid Isoleucine (Ile)) into *Ccrk* exon 3, the site between c.219 and c.220 (Figure 3A). As expected, CCRK expression was consistently upregulated by orthotopic RIL-175 inoculation in the BMs from *Ccrk*$^{indel/indel}$ and age-matched WT C57BL/6 mice but exhibited defective downstream p-STAT3^{Tyr705} expression (Figure 3B). To study if *Ccrk*$^{indel/indel}$ mice displayed impaired CCRK function in myeloid cells, we first repeated the MDSC-adoptive transfer experiment in a subcutaneous tumor model using BMs from WT and *Ccrk*$^{indel/indel}$ mice. To this end, C57BL/6 mice were inoculated by Hepa1-6 murine hepatoma stable cells with Ccrk-knockout (CrCcrk) generated by CRISPR/Cas9[2] and then intratumorally injected with BM-MDSCs from WT or *Ccrk*$^{indel/indel}$ mice described previously (Figure S3A). Of note, slower tumor growth rate as well as decreased endpoint tumor weights were observed in Hepa1-6-CrCcrk tumors receiving BM-MDSCs from *Ccrk*$^{indel/indel}$ mice compared WT ones (p < 0.01;

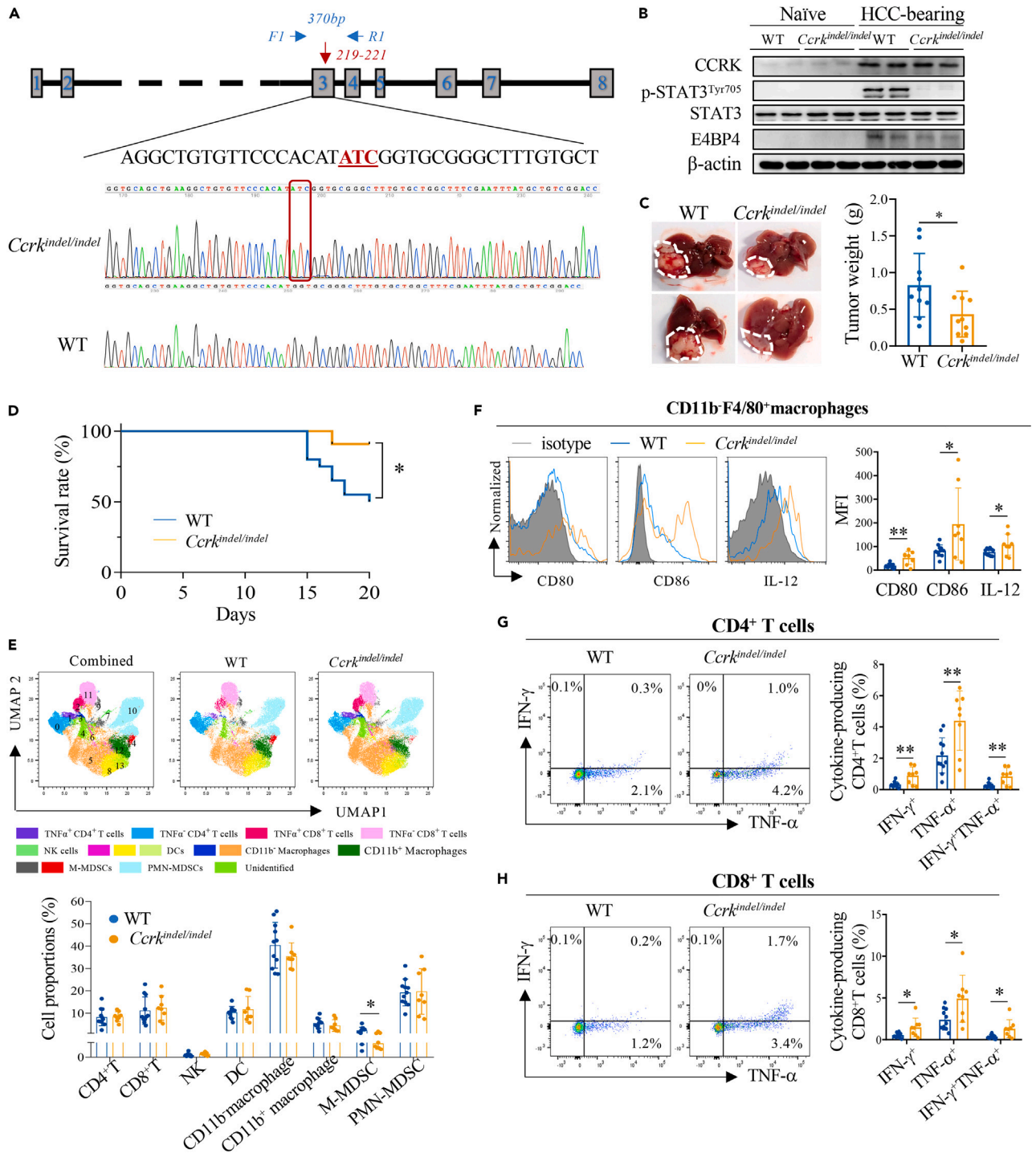

Figure 3. Inactivation of myeloid *Ccrk* reduces HCC progression by remodeling tumor microenvironment in orthotopic HCC mouse model

(A) DNA sequence of *Ccrk*$^{indel/indel}$ transgenic (TG) mouse. An ATC (encodes amino acid Ile) insertion in *Ccrk* exon 3 between c.219 and c.220 was generated in C57BL/6 mouse and confirmed by DNA sequencing.

(B) The expressions of CCRK, p-STAT3^{Tyr705}, STAT3 and E4BP4 in BMs of naive and RIL-175-tumor bearing wild-type (WT) and *Ccrk*$^{indel/indel}$ mice were detected by western blot. β-actin was served as loading control.

(C and D) (C) WT and *Ccrk*$^{indel/indel}$ mice were inoculated with 5*10^5 RIL-175 cells via intrahepatic injection and sacrificed at day 21 post tumor inoculation or humane endpoint (n ≥ 9). Liver tumor images and tumor weights at the endpoint are shown, and (D) their survival rates were documented.

Figure 3. *Continued*

(E) High-dimensional flow cytometry analysis in tumor-infiltrating CD45$^+$leukocytes are shown as visualization of clusters in UMAP plots for total and individual groups. UMAP plots shown consists of 40,000 cells each and are representative of concatenated samples within each group. Cell clusters corresponding to CD4$^+$ and CD8$^+$T cells, NK cells, DCs, macrophages, M-, and PMN-MDSCs are highlighted and their proportions in WT and *Ccrk*$^{indel/indel}$ mice are shown.

(F) Representative overlay histograms and mean fluorescence intensity (MFI) of CD80, CD86, and IL-12 expressions in CD11b$^-$ macrophages from WT and *Ccrk*$^{indel/indel}$ mice are shown.

(G and H) (G) Representative flow cytometry dot plots and proportions of IFN-γ$^+$, TNF-α$^+$, IFN-γ$^+$TNF-α$^+$CD4$^+$T cells or (H) CD8$^+$T cells in tumor-infiltrating CD45$^+$leukocytes from WT and *Ccrk*$^{indel/indel}$ mice are shown. Data are presented as mean ± SD. *, $p < 0.05$; **, $p < 0.01$.

See also Figures S3 and S4.

Figures S3B and S3C). In addition, when we inoculated RIL-175-tumor in *Ccrk*$^{indel/indel}$ mice and then intratumorally injected with BM-MDSCs from WT or *Ccrk*$^{indel/indel}$ mice (Figure S3D), we also observed that tumor growth rate and endpoint tumor weights were significantly reduced in tumors receiving BM-MDSCs from *Ccrk*$^{indel/indel}$ mice compared WT ones, which accompanied with increased tumor-infiltrating CD8$^+$T cells by immunofluorescence (IF) staining ($p < 0.05$; Figures S3E–S3G). Together, these data validated that the CCRK indel mutation resulted in *Ccrk* inactivation and dysfunction in MDSCs, independent of tumoral and host CCRK expression *in vivo*.

Finally, we determined the function of CCRK in MDSCs using the orthotopic HCC mouse model by intrahepatic injection of RIL-175 cells into WT and *Ccrk*$^{indel/indel}$ mice as previously.[30] Of note, *Ccrk*$^{indel/indel}$ mice displayed reduced endpoint tumor weights and improved survival when compared to WT controls ($p < 0.05$; Figures 3C and 3D). Interestingly, when we profiled the CD45$^+$TILs from WT and *Ccrk*$^{indel/indel}$ mice by high-dimensional flow cytometry (Figure 3E), we found that the TILs from *Ccrk*$^{indel/indel}$ mice contained decreased proportions of CD11b$^+$GR-1$^+$Ly6C$^+$ Ly6G$^-$M-MDSCs as well as increased expressions of maturation markers CD80, CD86 and IL-12 in CD11b$^-$F4/80$^+$macrophages, and IFN-γ$^+$ and/or TNF-α$^+$CD4$^+$ and CD8$^+$ T cells compared to WT controls ($p < 0.05$; Figures 3E–3H). Consistent increase of CD11b/Ly6C double-positive M-MDSCs but not of other cells was also verified in the tumors from *Ccrk*$^{indel/indel}$ mice by co-IF staining (Figure S4). As we have shown a myeloid-specific CCRK expression (Figures 1A and 1B) in RIL-175-bearing mice, these findings indicated that myeloid CCRK expression may function in maintaining the immunosuppressive features of TME to support orthotopic tumor progression *in vivo*.

CCRK knockdown reduces the immunosuppressive activity and induces an immune-stimulatory phenotype of myeloid cells

Since *CCRK* showed upregulation in patients with HCC (Figure 1C), we next explored the human relevance of our findings by generating MDSCs from human PBMCs (Figure S5A). As expected, CCRK expression was upregulated and accumulated in CD33$^+$HLA-DR$^-$MDSCs after 7-day culture in the presence of human recombinant IL-6/GM-CSF, compared to naive myeloid cell (MC) controls (Figure S5B). MDSCs were then purified by CD33 microbeads (Miltenyi Biotech) and treated with small interfering RNA (siRNA) against *CCRK* (si*CCRK*) or control siRNA (si*Ctrl*)[4] (Figure 4A). The knockdown efficiency of si*CCRK* was confirmed by qRT-PCR and western blot (Figure 4B). Since CCRK is regarded as a member of CDK family that drives cell proliferation,[29] MDSC proliferation rate was monitored by a carboxyfluorescein succinimidyl ester (CFSE) assay. Purified MDSCs were labeled with CFSE before si*Ctrl* or si*CCRK* transfection, and the cell proliferation rate indicated by CFSE intensity reduction was then measured at 3-day post siRNA treatment by flow cytometry (Figure 4A). The data showed that knockdown of *CCRK* significantly reduced the proliferation rate of MDSCs compared to si*Ctrl* ($p < 0.05$; Figure 4C), suggesting a potential role of CCRK in regulating MDSC expansion. Interestingly, further phenotypic analysis showed that MDSCs with lower CCRK expression have higher HLA-DR expression ($p < 0.01$; Figure 4D). Of note, the proportions of CD68$^+$HLA-DR$^+$ macrophages, which also highly expressed CD86 and CD80, were increased upon CCRK knockdown ($p < 0.05$; Figures 4E and 4F), consistent with our observations in the mouse models (Figures 2F, 2G, and 3F). These phenotypic changes suggested that CCRK depletion might prompt MDSC differentiation into mature macrophages with antigen presentation ability. Indeed, using a mixed lymphocyte reaction (MLR) assay (Figure 4A), we observed that si*CCRK*-treated MDSCs were more efficient in stimulating allogenic T cell proliferation and IFN-γ releasing when compared with si*Ctrl*-treated controls ($p < 0.05$; Figures 4G and 4H), which may be contributed by the decrease of MDSC proliferation rate and the increase of macrophage-like cells. Taken together, we concluded that CCRK is a key player functioning in the maintenance of immature and immunosuppressive status of MDSCs.

CCRK activates STAT3/E4BP4 transcriptional activity on *IL-10* induction and *IL-12* suppression in MDSCs

Previous studies have demonstrated that MDSCs exert their immunosuppression and maintain their immature status via soluble cytokines and proteins that are controlled by STAT3.[10] Since CCRK can induce STAT3 phosphorylation (Figures 2A and 3B), we next investigated potential functional mediators of CCRK/STAT3 pathway in MDSCs. Therefore, 11 soluble factors that are reported to function in regulating the immunosuppressive activity and differentiation of myeloid cell[1] were screened by qRT-PCR in si*Ctrl*- and si*CCRK* treated MDSCs. Besides *ARG-I*, knockdown of *CCRK* in MDSCs caused significant reduction of *IL-10*, and induction of *IL-12* ($p < 0.05$; Figure 5A), while other genes remained unchanged (*IFN-α*, *IFN-β*, *IL-1β*, *IL-6*, *IL-13*, *NOS2*, *TNF-α*, *TGF-β*) (Figure 5A). Consistent reduction in protein levels of IL-10 and ARG-I was also observed accompanied with *CCRK* knockdown in MDSCs by ELISA, western blot, and flow cytometry intracellular staining, respectively ($p < 0.01$; Figures 5B–5D). As important mediators in determining MDSC differentiation and functions, previous studies also demonstrated that (a) STAT3 can *trans*-activate *ARG-I* promoter to upregulate ARG-I in MDSCs; (b) IL-10 expression can be controlled by the transcription factor, E4 Promoter-Binding Protein 4 (E4BP4), in CD4$^+$ T cells; and (c) IL-12 expression can be transcriptionally suppressed by STAT3/E4BP4 through inhibition of its promoter or a distal enhancer.[11,31,32] Since we have found multiple STAT3 consensus binding

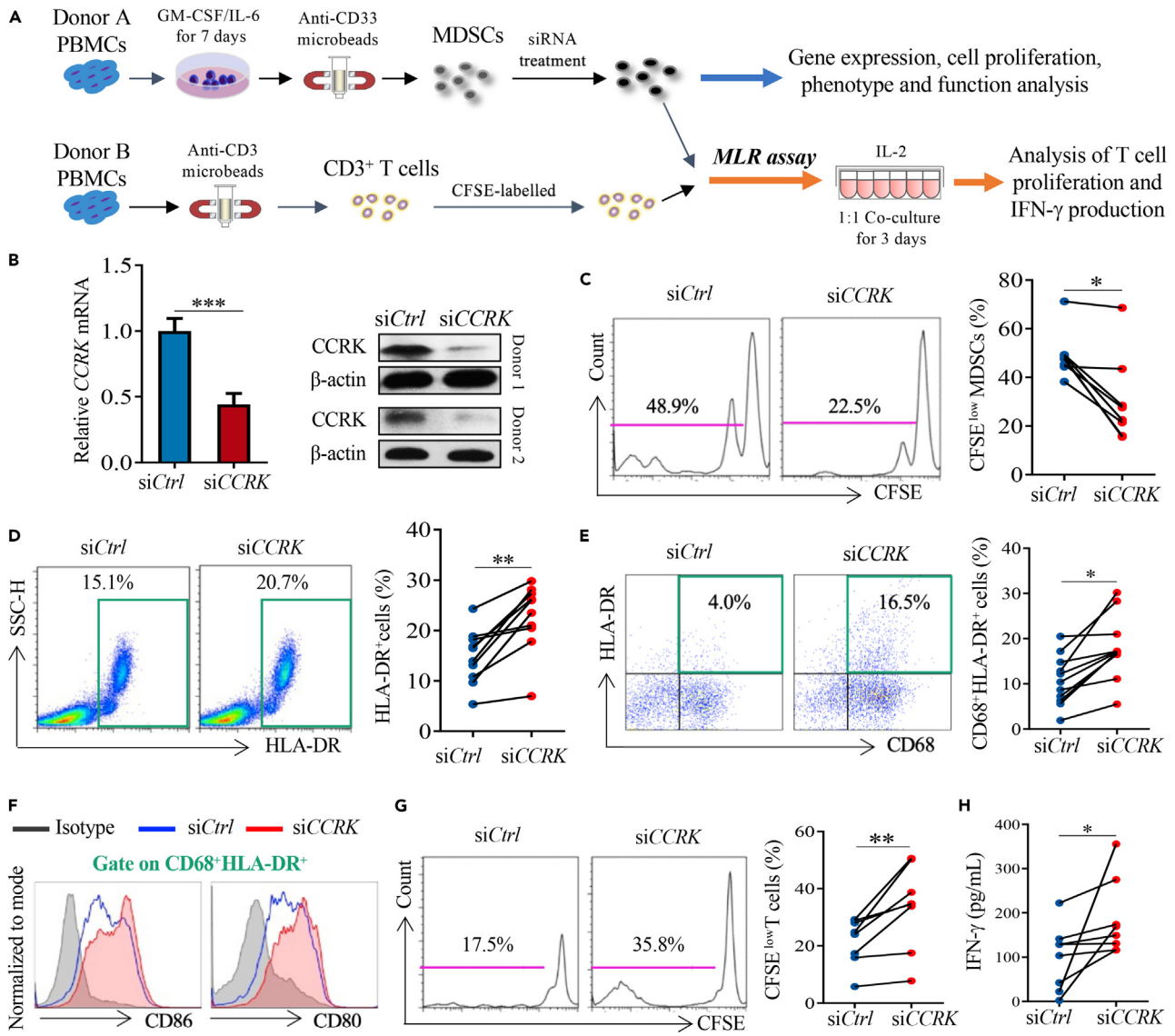

Figure 4. Knockdown of *CCRK* reduces the immunosuppressive activity and induces an immune-stimulatory phenotype of MDSCs

(A) Schematic diagram. CD33$^+$MDSCs were generated from healthy donor PBMCs treated with IL-6/GM-CSF for seven days and purified by CD33 microbeads. Purified MDSCs were transfected with siRNA targeting CCRK (si*CCRK*) or control (si*Ctrl*). Cells were collected and analyzed by qRT-PCR, western blot, or flow cytometry. The antigen-presenting capacity of MDSCs treated with siRNA was determined by mixed leukocyte reaction (MLR) assay via co-culturing them with CD3 microbeads purified and CFSE-labeled CD3$^+$T cells from a different donor, at a ratio of 1:1 in the presence of human recombinant IL-2 (20 U/mL). T cell proliferation rate and IFN-γ releasing were analyzed by flow cytometry and ELISA, respectively.

(B) CCRK expressions in MDSCs treated with si*Ctrl* or si*CCRK* are shown at mRNA (relative to *GAPDH*) and protein levels. β-actin was served as loading control. Data are presented as mean ± SD from at least five independent experiments.

(C) MDSCs labeled with CFSE before siRNA treatment were used to measure MDSC proliferation and CFSE^{low} cells indicated the proliferating population was analyzed by flow cytometry at day three post transfection.

(D–F) (D) The expressions of HLA-DR, (E) proportions of CD68$^+$HLA-DR$^+$ macrophages, as well as (F) CD86 and CD80 surface expressions on CD68$^+$HLA-DR$^+$ macrophages were upregulated upon *CCRK* knockdown in MDSCs.

(G and H) (G) MLR assay showed an up-regulated allogenic T cell proliferation indicated by CFSE^{low} proportion and (H) IFN-γ production in T cells co-cultured with MDSC-si*CCRK* compared to controls. (n = 7). *p < 0.05, **p < 0.01, ***p < 0.001.

See also Figure S5.

sequences in the *E4BP4* promoter region, we hypothesized that CCRK may activate STAT3 to control E4BP4 transcriptional activity in MDSCs. We thus examined the expression and activity of STAT3 and E4BP4 in MDSCs treated with si*Ctrl* or si*CCRK*. As expected, CCRK ablation in MDSCs resulted in significant decrease of total STAT3 as well as p-STAT3^{Tyr705} detected by qRT-PCR, western blot, and flow cytometry

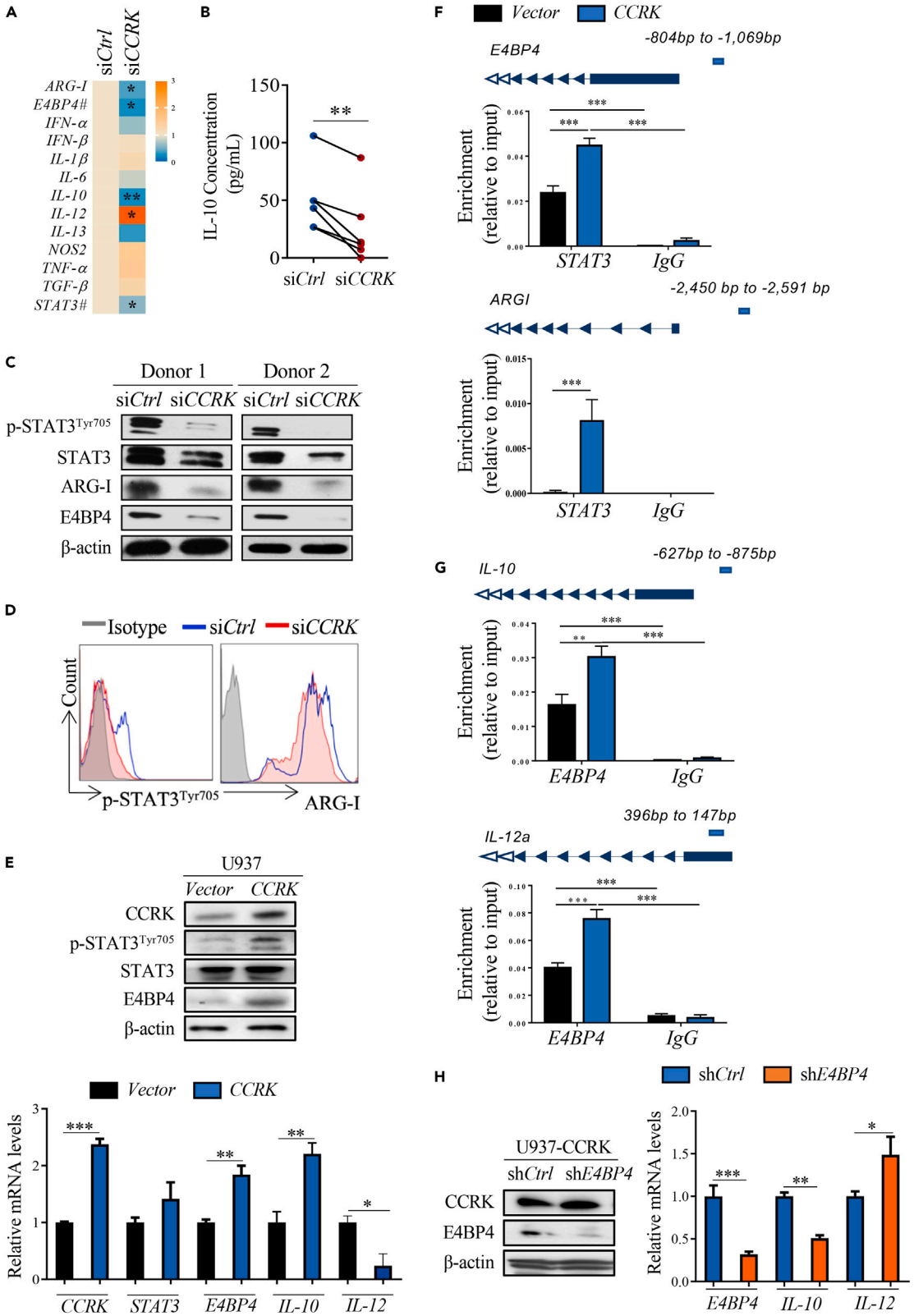
A
siCtrl
siCCRK
ARG-I
E4BP4#
IFN-α
IFN-β
IL-1β
IL-6
IL-10
IL-12
IL-13
NOS2
TNF-α
TGF-β
STAT3#
B
IL-10 Concentration (pg/mL)
siCtrl siCCRK
C
Donor 1
Donor 2
siCtrl siCCRK siCtrl siCCRK
p-STAT3Tyr705
STAT3
ARG-I
E4BP4
β-actin
D
Isotype
siCtrl
siCCRK
Count
p-STAT3Tyr705
ARG-I
E
U937
Vector CCRK
CCRK
p-STAT3Tyr705
STAT3
E4BP4
β-actin
Vector
CCRK
Relative mRNA levels
CCRK
STAT3
E4BP4
IL-10
IL-12
F
Vector
CCRK
E4BP4
-804bp to -1,069bp
Enrichment (relative to input)
STAT3
IgG
ARGI
-2,450 bp to -2,591 bp
G
IL-10
-627bp to -875bp
IL-12a
396bp to 147bp
H
shCtrl
shE4BP4
U937-CCRK
shCtrl shE4BP4
CCRK
E4BP4
β-actin
Relative mRNA levels
E4BP4
IL-10
IL-12

Figure 5. CCRK activates STAT3/E4BP4-dependent transcriptional regulation to maintain the *IL-10/IL-12* balance in myeloid cells

(A) CD33^{+}MDSCs were generated, purified, and transfected with si*Ctrl* or si*CCRK*. The mRNA levels of 13 genes (relative to *GAPDH*) determined by qRT-PCR are shown in heatmap.

(B and C) (B) IL-10 level, (C) protein expressions of p-STAT3^{Tyr705}, STAT3, ARG-I, and E4BP4 were detected in si*Ctrl*- or si*CCRK*-treated MDSCs at 48-h by ELISA or western blot, respectively.

(D) The expressions of p-STAT3^{Tyr705} and ARG-I in si*Ctrl*- or si*CCRK*-treated MDSCs were further confirmed by intracellular flow cytometry analysis and are shown in overlay histograms.

(E) Western blot analysis of CCRK, p-STAT3^{Tyr705}, STAT3 and E4BP4, and qRT-PCR analysis of *CCRK*, *E4BP4*, *IL-10*, and *IL-12* mRNA levels (relative to *GAPDH*) in vector- or CCRK-U937 stable cells.

(F and G) (F) qChIP-PCR analyses of STAT3 on *E4BP4* and *ARGI* promoters, and (G) E4BP4 on the promoters of *IL-10* and *IL-12a* in vector- or CCRK-U937 stable cells. The promoter regions for TF binding of indicated genes are shown.

(H) Western blot analysis of CCRK and E4BP4, and qRT-PCR analysis of *E4BP4*, *IL-10* and *IL-12* mRNA levels (relative to *GAPDH*) in U937-CCRK cells treated by sh*Ctrl* or sh*E4BP4* are shown. β-actin was served as loading control. Data are presented as mean ± SD from at least five independent experiments. *$p < 0.05$, **$p < 0.01$, ***$p < 0.001$.

See also Figure S6.

intracellular staining, respectively (Figure 5A, 5C, and 5D). In parallel, the reduction of E4BP4 in both mRNA and protein levels was observed in si*CCRK*-treated MDSCs compared to control ($p < 0.05$; Figures 5A and 5C). Consistent E4BP4 upregulation was detected in mouse BM-MDSCs compared to IMC (Figure S1), which could be suppressed by LV-sh*Ccrk* infection or *CCRK* indel mutation (Figures 2A and 3B). Moreover, treatment of MDSCs with a STAT3 inhibitor, Stattic (10 μM) not only abolished STAT3 phosphorylation, but also reduced the expressions of both ARG-I and E4BP4 ($p < 0.05$; Figures S6A and S6B). In parallel, *IL-10* was decreased, while *IL-12* was increased ($p < 0.05$; Figure S6A), suggesting that STAT3 may be the upstream of E4BP4 in MDSCs. To further confirm the importance of this pathway, we constructed a CCRK-expressed stable cell line using human myeloid cell U937, in which ectopic CCRK expression upregulated p-STAT3^{Tyr705}, E4BP4 and *IL-10* and decreased *IL-12* expressions, but not total STAT3 expression (Figure 5E). qChIP-PCR analysis in this CCRK-U937 stable cells showed that CCRK induced a significantly increased occupancy of STAT3 in the promoter region of *E4BP4* and *ARGI* ($p < 0.001$; Figure 5F). The upregulated E4BP4 could then bind to the promoter regions of *IL-10* and *IL-12a*, which in turn control their transcription in CCRK-expressed, but not vector-control U937 cells ($p < 0.01$; Figure 5G). Knockdown of E4BP4 by a lentivirus-based shRNA approach could therefore decrease *IL-10* expression and increase *IL-12* expression in CCRK-expressed U937 cells ($p < 0.05$; Figure 5H). Since the balance of ARG-I/IL-10/IL-12 has been demonstrated to determine myeloid cell identity and functions, our findings pinpointed a possible molecular mechanism of why CCRK is important in MDSCs.

DISCUSSION

Accumulating evidence from preclinical and clinical studies suggests that myeloid cell status and function determine the immunosuppressive nature of TME.[1] MDSCs are one of the earliest infiltrating cells in HCC tumors that associated with disease progression, recurrence, metastasis, and poor prognosis as well as immunotherapy resistance.[3] Accordingly, therapeutic approaches aimed at inhibiting MDSC expansion and recruitment, depleting MDSCs directly or reprograming them toward an immune-stimulatory phenotype have shown great potential in both pre-clinical HCC models[10] and clinical trials (NCT04123379; NCT02868255; NCT01839604). Here, we identified myeloid CCRK activation as a critical determinator of myeloid cell-mediated immunosuppression and tumor progression. Knockdown or genetic inactivation of *CCRK* in myeloid cells restricted tumor growth by skewing myeloid cell toward a mature and immune-stimulatory status. These changes in turn potentiated T cell responses and a dramatic shift toward a TME enriched with cytolytic cytokines like IFN-γ and TNF-α. Mechanistically, CCRK upregulation triggered STAT3/E4BP4 transcriptional activity to maintain immunosuppressive features of MDSCs. As our previous findings also showed CCRK overexpression in human HCCs with MDSC abundance,[4,5] we surmise that inhibition of CCRK offers an opportunity to simultaneously suppress hepatoma intrinsic oncogenic signaling and reprogram immune-suppressive myeloid cells for HCC therapy.

As fundamental drivers of cell cycle that are required for the initiation and progression of various malignancies, CDKs have long been regarded as promising therapeutic targets in cancers.[17] Accordingly, pharmacological inhibition of CDKs has produced promising results in clinical trials.[17] Mechanistic studies showed that CDKs blockade contributes to tumor suppression not only by directly dysregulating tumor cell cycle, but also indirectly through orchestrating immune cell fate and function. For example, inhibition of CDK4/6 expressed in T cells enhances T cell activation to augment anti-tumor immunity by increasing IL-2 secretion, which in turn largely improves the clinical benefits of combined CDK4/6 inhibitors and immunotherapy approaches.[33,34] In line with these findings, our data pinpointed that the expression of the latest CDK family member, CDK20 or CCRK can be induced in tumor-bearing hosts, which function in regulating the proliferation, expansion, and immunosuppression of MDSCs. More importantly, suppression of myeloid CCRK disrupted the immunosuppressive TME with enhanced T cell cytotoxicity, thus inhibiting tumor progression and prolonging mouse survival. As high levels of MDSCs are demonstrated to be associated with resistance to chemotherapy and immunotherapy in HCC patients,[10,30] further studies are needed to explore the therapeutic efficacy of combined approaches with myeloid CCRK inhibition.

Our group has previously reported that the pro-inflammatory IL-6/STAT3 and androgen receptor (AR) signaling could directly induce CCRK transcription in hepatoma cells, which in turn activate the oncogenic β-catenin/mTORC/NF-κB signaling to promote tumor proliferation and immunosuppression.[4,23–25] Interestingly, our preliminary data suggested that IL-6 may also upregulate CCRK expression in MDSCs independent of p-STAT3, highlighting the difference in CCRK signals between HCC and MDSCs. Indeed, we discovered a myeloid cell-intrinsic CCRK

pathway by inducing STAT3 phosphorylation to trigger E4BP4-dependent transcriptional regulation in this study. Originally identified as a key transcription factor in regulating the differentiation and function of NK,[35] further studies reported that E4BP4 also has multiple functions in controlling the plasticity of $CD4^{+}$T cells and NKT cells by transcriptional regulating *IL-10* and *IL-13* expression.[31] In addition, Smith et al. uncovered that E4BP4 transcriptionally represses *IL-12* expression in myeloid cells under the stimulation by IL-10/IL-10R.[32] The balance of IL-10/IL-12 could therefore control the transition between immunosuppressive state and immune activation, through modulating Tregs or the maturation of macrophages and DCs in TME.[36] Our current study further revealed that E4BP4 could be activated by the CCRK/STAT3 pathway and maintains the immature and suppressive status of MDSCs via control of IL-10/IL-12 balance. However, whether CCRK/E4BP4 may control MDSC phenotypes and immunosuppression via additional downstream factors needs further investigation. In addition, how CCRK regulates STAT3 phosphorylation and which factors derived from tumor cells may contribute to the activation of CCRK/E4BP4 in myeloid cells are also unknown, requiring further studies on the molecular basic of CCRK signal are needed.

Previous studies by us and others have demonstrated the consistent overexpression of CCRK in cancers arising from brain, colon, liver, lung, and ovary correlates with tumor staging, shorter patient survival, and poor prognosis.[29] However, the development of CCRK-specific inhibitors is still under challenging exploration. A major reason for this is, perhaps, the identification of key effective domains in CCRK protein. Using the established $Ccrk^{indel/indel}$ TG mice, we pinpointed the importance of exon 3 in determining myeloid CCRK function. The altered protein sequence by the insertion of amino acid Ile in exon 3 may be essential to maintain a functional structure and kinase activity of CCRK, which may provide proof-of-concept for the development of CCRK inhibitors for *in vivo* use. As MDSC abundance is widely reported to regulated tumor immunosuppression and associate with immunotherapy resistance in various cancers,[10,12,30,37–39] our data highlights the multiple facets of CCRK in promoting tumor immunosuppression and hepatic carcinogenesis. Importantly, CCRK is a highly druggable target, with clear opportunities for structure-based drug design and as such represents an eminently exploitable target for MDSCs in HCC as well as other cancers.

Limitations of the study

One of the limitations of the current study is the orthotopic mouse model using hepatoma cell line. We are aware that insights from the orthotopic HCC mouse model may not fully recapitulate the heterogeneous features in TME and have provided limited prediction for the outcomes in clinic. Since CCRK is highly expressed by both hepatoma and tumor-associated myeloid cells to maintain tumor immunosuppression, developing, and evaluating the therapeutic potential of CCRK-specific targeted agents, either in single or combinatory immunotherapy should be necessary for further investigation. Additionally, considerable evidence on the role of CCRK in MDSCs has been generated by genetic deletion models and it will be important to confirm these findings with suitable chemical tool inhibitors when these become available in the future.

STAR★METHODS

Detailed methods are provided in the online version of this paper and include the following:

- KEY RESOURCES TABLE
- RESOURCE AVAILABILITY
  - Lead contact
  - Materials availability
  - Data and code availability
- EXPERIMENTAL MODEL AND STUDY PARTICIPANT DETAILS
  - Patient specimens
  - Cell lines
  - Mice
- METHOD DETAILS
  - Single cell isolation and flow cytometry analysis
  - Quantitative RT-PCR
  - Western blot
  - Mouse BM-derived MDSCs
  - Lentivirus preparation and infection
  - Generation of $Ccrk^{indel/indel}$ transgenic (TG) mouse
  - *In vivo* experiments
  - Human MDSC proliferation and differentiation assays
  - Mixed lymphocyte reaction (MLR) assay
  - Chromatin immunoprecipitation-quantitative PCR (ChIP-qPCR)
  - Immunofluorescence staining
- QUANTIFICATION AND STATISTICAL ANALYSIS

SUPPLEMENTAL INFORMATION

Supplemental information can be found online at https://doi.org/10.1016/j.isci.2023.107626.

ACKNOWLEDGMENTS

We thank Prof. Tim F. Greten (National Cancer Institute, National Institutes of Health, Bethesda, USA) and Prof. Lars Zender (University Hospital Tubingen, Germany) for providing us with RIL175 cell line. We thank Prof. Nathaniel R. Landau (New York University School of Medicine) for providing us the backbone plasmids used for lentivirus construction. We thank Prof. Alex N. Bullock (University of Oxford, United Kingdom) for helpful discussions. This project is supported by the University Grants Committee through General Research Fund (14108219, 14115820, 14120621), Collaborative Research Fund (C4045-18W), the Li Ka Shing Foundation, the Strategic Seed Funding for Collaborative Research Scheme (2021-22), and the Health and Medical Research Fund (03141376; 07180556).

AUTHOR CONTRIBUTIONS

Conceptualization, J.Z., and A.S.L.C.; Methodology, J.Z., H.W., T.S., J.W., W.Y., J.L., L.D., M.L., H.S.; Paper writing and review: J.Z., S.E.W., and A.S.L.C.; Resources, J.W., P.B.L; Transgenic mouse construction, S.W.T., K.L.C; Supervision, J.Z., and A.S.L.C., Funding Acquisition, J.Z., J.J.S., and A.S.L.C.

DECLARATION OF INTERESTS

The authors declare no competing interests that pertain to this work except the following declaration. J.Z., and A.S.L.C. hold a related US Provisional Patent (Application No: 63/528,199).

INCLUSION AND DIVERSITY

We support inclusive, diverse, and equitable conduct of research.

Received: January 18, 2023
Revised: June 16, 2023
Accepted: August 9, 2023
Published: August 12, 2023

REFERENCES

1. Veglia, F., Sanseviero, E., and Gabrilovich, D.I. (2021). Myeloid-derived suppressor cells in the era of increasing myeloid cell diversity. Nat. Rev. Immunol. *21*, 485–498. https://doi.org/10.1038/s41577-020-00490-y.
2. De Henau, O., Rausch, M., Winkler, D., Campesato, L.F., Liu, C., Cymerman, D.H., Budhu, S., Ghosh, A., Pink, M., Tchaicha, J., et al. (2016). Overcoming resistance to checkpoint blockade therapy by targeting PI3Kgamma in myeloid cells. Nature *539*, 443–447. https://doi.org/10.1038/nature20554.
3. Wan, S., Kuo, N., Kryczek, I., Zou, W., and Welling, T.H. (2015). Myeloid cells in hepatocellular carcinoma. Hepatology *62*, 1304–1312. https://doi.org/10.1002/hep.27867.
4. Zhou, J., Liu, M., Sun, H., Feng, Y., Xu, L., Chan, A.W.H., Tong, J.H., Wong, J., Chong, C.C.N., Lai, P.B.S., et al. (2018). Hepatoma-intrinsic CCRK inhibition diminishes myeloid-derived suppressor cell immunosuppression and enhances immune-checkpoint blockade efficacy. Gut *67*, 931–944. https://doi.org/10.1136/gutjnl-2017-314032.
5. Liu, M., Zhou, J., Liu, X., Feng, Y., Yang, W., Wu, F., Cheung, O.K.W., Sun, H., Zeng, X., Tang, W., et al. (2020). Targeting monocyte-intrinsic enhancer reprogramming improves immunotherapy efficacy in hepatocellular carcinoma. Gut *69*, 365–379. https://doi.org/10.1136/gutjnl-2018-317257.
6. Veltman, J.D., Lambers, M.E.H., van Nimwegen, M., Hendriks, R.W., Hoogsteden, H.C., Aerts, J.G.J.V., and Hegmans, J.P.J.J. (2010). COX-2 inhibition improves immunotherapy and is associated with decreased numbers of myeloid-derived suppressor cells in mesothelioma. Celecoxib influences MDSC function. BMC Cancer *10*, 464. https://doi.org/10.1186/1471-2407-10-464.
7. Rodriguez, P.C., Hernandez, C.P., Quiceno, D., Dubinett, S.M., Zabaleta, J., Ochoa, J.B., Gilbert, J., and Ochoa, A.C. (2005). Arginase I in myeloid suppressor cells is induced by COX-2 in lung carcinoma. J. Exp. Med. *202*, 931–939. https://doi.org/10.1084/jem.20050715.
8. Bauer, R., Udonta, F., Wroblewski, M., Ben-Batalla, I., Santos, I.M., Taverna, F., Kuhlencord, M., Gensch, V., Päsler, S., Vinckier, S., et al. (2018). Blockade of Myeloid-Derived Suppressor Cell Expansion with All-Trans Retinoic Acid Increases the Efficacy of Antiangiogenic Therapy. Cancer Res. *78*, 3220–3232. https://doi.org/10.1158/0008-5472.CAN-17-3415.
9. Michels, T., Shurin, G.V., Naiditch, H., Sevko, A., Umansky, V., and Shurin, M.R. (2012). Paclitaxel promotes differentiation of myeloid-derived suppressor cells into dendritic cells *in vitro* in a TLR4-independent manner. J. Immunot. *9*, 292–300. https://doi.org/10.3109/1547691X.2011.642418.
10. Li, K., Shi, H., Zhang, B., Ou, X., Ma, Q., Chen, Y., Shu, P., Li, D., and Wang, Y. (2021). Myeloid-derived suppressor cells as immunosuppressive regulators and therapeutic targets in cancer. Signal Transduct. Targeted Ther. *6*, 362. https://doi.org/10.1038/s41392-021-00670-9.
11. Vasquez-Dunddel, D., Pan, F., Zeng, Q., Gorbounov, M., Albesiano, E., Fu, J., Blosser, R.L., Tam, A.J., Bruno, T., Zhang, H., et al. (2013). STAT3 regulates arginase-I in myeloid-derived suppressor cells from cancer patients. J. Clin. Invest. *123*, 1580–1589. https://doi.org/10.1172/JCI60083.
12. Trovato, R., Fiore, A., Sartori, S., Canè, S., Giugno, R., Cascione, L., Paiella, S., Salvia, R., De Sanctis, F., Poffe, O., et al. (2019). Immunosuppression by monocytic myeloid-derived suppressor cells in patients with pancreatic ductal carcinoma is orchestrated by STAT3. J. Immunother. Cancer *7*, 255. https://doi.org/10.1186/s40425-019-0734-6.
13. Kumar, V., Cheng, P., Condamine, T., Mony, S., Languino, L.R., McCaffrey, J.C., Hockstein, N., Guarino, M., Masters, G., Penman, E., et al. (2016). CD45 Phosphatase Inhibits STAT3 Transcription Factor Activity in Myeloid Cells and Promotes Tumor-Associated Macrophage Differentiation. Immunity *44*, 303–315. https://doi.org/10.1016/j.immuni.2016.01.014.
14. Nefedova, Y., Nagaraj, S., Rosenbauer, A., Muro-Cacho, C., Sebti, S.M., and Gabrilovich, D.I. (2005). Regulation of dendritic cell differentiation and antitumor immune response in cancer by pharmacologic-selective inhibition of the janus-activated kinase 2/signal transducers and activators of transcription 3 pathway. Cancer Res. *65*, 9525–9535. https://doi.org/10.1158/0008-5472.CAN-05-0529.
15. Reilley, M.J., McCoon, P., Cook, C., Lyne, P., Kurzrock, R., Kim, Y., Woessner, R., Younes, A., Nemunaitis, J., Fowler, N., et al. (2018). STAT3 antisense oligonucleotide AZD9150 in a subset of patients with heavily pretreated lymphoma: results of a phase 1b trial. J. Immunother. Cancer *6*, 119. https://doi.org/10.1186/s40425-018-0436-5.
16. Milner, J.D., Brenchley, J.M., Laurence, A., Freeman, A.F., Hill, B.J., Elias, K.M., Kanno, Y., Spalding, C., Elloumi, H.Z., Paulson, M.L., et al. (2008). Impaired T(H)17 cell differentiation in subjects with autosomal

dominant hyper-IgE syndrome. Nature *452*, 773–776. https://doi.org/10.1038/nature06764.

17. Asghar, U., Witkiewicz, A.K., Turner, N.C., and Knudsen, E.S. (2015). The history and future of targeting cyclin-dependent kinases in cancer therapy. Nat. Rev. Drug Discov. *14*, 130–146. https://doi.org/10.1038/nrd4504.
18. Wells, A.D., and Morawski, P.A. (2014). New roles for cyclin-dependent kinases in T cell biology: linking cell division and differentiation. Nat. Rev. Immunol. *14*, 261–270. https://doi.org/10.1038/nri3625.
19. Heckler, M., Ali, L.R., Clancy-Thompson, E., Qiang, L., Ventre, K.S., Lenehan, P., Roehle, K., Luoma, A., Boelaars, K., Peters, V., et al. (2021). Inhibition of CDK4/6 Promotes CD8 T-cell Memory Formation. Cancer Discov. *11*, 2564–2581. https://doi.org/10.1158/2159-8290.CD-20-1540.
20. Morawski, P.A., Mehra, P., Chen, C., Bhatti, T., and Wells, A.D. (2013). Foxp3 protein stability is regulated by cyclin-dependent kinase 2. J. Biol. Chem. *288*, 24494–24502. https://doi.org/10.1074/jbc.M113.467704.
21. Goel, S., DeCristo, M.J., Watt, A.C., BrinJones, H., Sceneay, J., Li, B.B., Khan, N., Ubellacker, J.M., Xie, S., Metzger-Filho, O., et al. (2017). CDK4/6 inhibition triggers anti-tumour immunity. Nature *548*, 471–475. https://doi.org/10.1038/nature23465.
22. Leitch, A.E., Lucas, C.D., Marwick, J.A., Duffin, R., Haslett, C., and Rossi, A.G. (2012). Cyclin-dependent kinases 7 and 9 specifically regulate neutrophil transcription and their inhibition drives apoptosis to promote resolution of inflammation. Cell Death Differ. *19*, 1950–1961. https://doi.org/10.1038/cdd.2012.80.
23. Feng, H., Cheng, A.S.L., Tsang, D.P., Li, M.S., Go, M.Y., Cheung, Y.S., Zhao, G.J., Ng, S.S., Lin, M.C., Yu, J., et al. (2011). Cell cycle-related kinase is a direct androgen receptor-regulated gene that drives beta-catenin/T cell factor-dependent hepatocarcinogenesis. J. Clin. Invest. *121*, 3159–3175. https://doi.org/10.1172/JCI45967.
24. Feng, H., Yu, Z., Tian, Y., Lee, Y.Y., Li, M.S., Go, M.Y.Y., Cheung, Y.S., Lai, P.B.S., Chan, A.M.L., To, K.F., et al. (2015). A CCRK-EZH2 epigenetic circuitry drives hepatocarcinogenesis and associates with tumor recurrence and poor survival of patients. J. Hepatol. *62*, 1100–1111. https://doi.org/10.1016/j.jhep.2014.11.040.
25. Zeng, X., Zhou, J., Xiong, Z., Sun, H., Yang, W., Mok, M.T.S., Wang, J., Li, J., Liu, M., Tang, W., et al. (2021). Cell cycle-related kinase reprograms the liver immune microenvironment to promote cancer metastasis. Cell. Mol. Immunol. *18*, 1005–1015. https://doi.org/10.1038/s41423-020-00534-2.
26. Sun, H., Yang, W., Tian, Y., Zeng, X., Zhou, J., Mok, M.T.S., Tang, W., Feng, Y., Xu, L., Chan, A.W.H., et al. (2018). An inflammatory-CCRK circuitry drives mTORC1-dependent metabolic and immunosuppressive reprogramming in obesity-associated hepatocellular carcinoma. Nat. Commun. *9*, 5214. https://doi.org/10.1038/s41467-018-07402-8.
27. Zender, L., Xue, W., Cordón-Cardo, C., Hannon, G.J., Lucito, R., Powers, S., Flemming, P., Spector, M.S., and Lowe, S.W. (2005). Generation and analysis of genetically defined liver carcinomas derived from bipotential liver progenitors. Cold Spring Harbor Symp. Quant. Biol. *70*, 251–261. https://doi.org/10.1101/sqb.2005.70.059.
28. Bobadilla, S., Sunseri, N., and Landau, N.R. (2013). Efficient transduction of myeloid cells by an HIV-1-derived lentiviral vector that packages the Vpx accessory protein. Gene Ther. *20*, 514–520. https://doi.org/10.1038/gt.2012.61.
29. Mok, M.T., Zhou, J., Tang, W., Zeng, X., Oliver, A.W., Ward, S.E., and Cheng, A.S. (2018). CCRK is a novel signalling hub exploitable in cancer immunotherapy. Pharmacol. Ther. *186*, 138–151. https://doi.org/10.1016/j.pharmthera.2018.01.008.
30. Kwong, T.T., Wong, C.H., Zhou, J.Y., Cheng, A.S.L., Sung, J.J.Y., Chan, A.W.H., and Chan, S.L. (2021). Chemotherapy-induced recruitment of myeloid-derived suppressor cells abrogates efficacy of immune checkpoint blockade. JHEP Rep. *3*, 100224. https://doi.org/10.1016/j.jhepr.2020.100224.
31. Motomura, Y., Kitamura, H., Hijikata, A., Matsunaga, Y., Matsumoto, K., Inoue, H., Atarashi, K., Hori, S., Watarai, H., Zhu, J., et al. (2011). The transcription factor E4BP4 regulates the production of IL-10 and IL-13 in CD4+ T cells. Nat. Immunol. *12*, 450–459. https://doi.org/10.1038/ni.2020.
32. Smith, A.M., Qualls, J.E., O'Brien, K., Balouzian, L., Johnson, P.F., Schultz-Cherry, S., Smale, S.T., and Murray, P.J. (2011). A distal enhancer in Il12b is the target of transcriptional repression by the STAT3 pathway and requires the basic leucine zipper (B-ZIP) protein NFIL3. J. Biol. Chem. *286*, 23582–23590. https://doi.org/10.1074/jbc.M111.249235.
33. Lelliott, E.J., Sheppard, K.E., and McArthur, G.A. (2022). Harnessing the immunotherapeutic potential of CDK4/6 inhibitors in melanoma: is timing everything? npj Precis. Oncol. *6*, 26. https://doi.org/10.1038/s41698-022-00273-9.
34. Deng, J., Wang, E.S., Jenkins, R.W., Li, S., Dries, R., Yates, K., Chhabra, S., Huang, W., Liu, H., Aref, A.R., et al. (2018). CDK4/6 Inhibition Augments Antitumor Immunity by Enhancing T-cell Activation. Cancer Discov. *8*, 216–233. https://doi.org/10.1158/2159-8290.CD-17-0915.
35. Gascoyne, D.M., Long, E., Veiga-Fernandes, H., de Boer, J., Williams, O., Seddon, B., Coles, M., Kioussis, D., and Brady, H.J.M. (2009). The basic leucine zipper transcription factor E4BP4 is essential for natural killer cell development. Nat. Immunol. *10*, 1118–1124. https://doi.org/10.1038/ni.1787.
36. Lin, W.W., and Karin, M. (2007). A cytokine-mediated link between innate immunity, inflammation, and cancer. J. Clin. Invest. *117*, 1175–1183. https://doi.org/10.1172/JCI31537.
37. Görgün, G.T., Whitehill, G., Anderson, J.L., Hideshima, T., Maguire, C., Laubach, J., Raje, N., Munshi, N.C., Richardson, P.G., and Anderson, K.C. (2013). Tumor-promoting immune-suppressive myeloid-derived suppressor cells in the multiple myeloma microenvironment in humans. Blood *121*, 2975–2987. https://doi.org/10.1182/blood-2012-08-448548.
38. Stromnes, I.M., Brockenbrough, J.S., Izeradjene, K., Carlson, M.A., Cuevas, C., Simmons, R.M., Greenberg, P.D., and Hingorani, S.R. (2014). Targeted depletion of an MDSC subset unmasks pancreatic ductal adenocarcinoma to adaptive immunity. Gut *63*, 1769–1781. https://doi.org/10.1136/gutjnl-2013-306271.
39. Tan, Z., Liu, L., Chiu, M.S., Cheung, K.W., Yan, C.W., Yu, Z., Lee, B.K., Liu, W., Man, K., and Chen, Z. (2019). Virotherapy-recruited PMN-MDSC infiltration of mesothelioma blocks antitumor CTL by IL-10-mediated dendritic cell suppression. OncoImmunology *8*, e1518672. https://doi.org/10.1080/2162402X.2018.1518672.

STAR★METHODS

KEY RESOURCES TABLE

REAGENT or RESOURCE	SOURCE	IDENTIFIER
Antibodies		
PerCP-Cyanine5.5 anti-mouse CD11b (clone M1/70)	Thermo Fisher Scientific	45-0112-82; RRID:AB_953558
PE anti-mouse CD11b (clone M1/70)	Thermo Fisher Scientific	12-0112-82; RRID:AB_2734869
APC-eFluor 780 anti-mouse CD11c (clone N418)	Thermo Fisher Scientific	47-0114-82; RRID:AB_1548652
BUV563 anti-mouse CD11c (clone N418)	BD Biosciences	749040; RRID:AB_2873434
APC anti-mouse CD3e (clone 145-2C11)	Thermo Fisher Scientific	17-0031-82; RRID:AB_469315
BB755 anti-mouse CD4 (clone RM4-5)	BD Biosciences	624391
Brilliant Violet 711™ anti-mouse CD45 (clone 30-F11)	Biolegend	103147; RRID:AB_2564383
Brilliant Ultra Violet™ 805 anti-mouse CD45 (clone 30-F11)	Thermo Fisher Scientific	368-0451-82; RRID:AB_2896112
FITC anti-mouse CD80 (clone 16-10A1)	Thermo Fisher Scientific	11-0801-82; RRID:AB_465133
BV421 anti-mouse CD80 (clone 16-10A1)	BD Biosciences	562611; RRID:AB_2737675
PE-CF594 anti-mouse CD86 (clone GL1)	BD Biosciences	567592; RRID:AB_2916657
PerCP/Cyanine5.5 anti-mouse CD86 (clone GL1)	Biolegend	105028; RRID:AB_2074994
BB790 anti-mouse CD8a (clone 53-6.7)	BD Biosciences	624296
APC-eFluor 780 anti-mouse CD8a (clone 53-6.7)	Thermo Fisher Scientific	47-0081-82; RRID:AB_1272185
BUV395 anti-mouse F4/80 (clone T45-2342)	BD Biosciences	565614; RRID:AB_2739304
BUV737 anti-mouse Ly-6G and Ly-6C (Gr-1) (clone RB6-8c5)	BD Biosciences	741712; RRID:AB_2871086
PE/Cyanine5 anti-mouse Ly-6G/Ly-6C (Gr-1) (clone RB6-8c5)	Biolegend	108410; RRID:AB_313375
UV440 fixable Viability Stain	BD Biosciences	566332; RRID:AB_2869748
BV605 anti-mouse Ly-6C (clone AL-21)	BD Biosciences	563011; RRID:AB_2737949
BV510 anti-mouse Ly-6G (clone 1A8)	BD Biosciences	740157; RRID:AB_2739910
BB660 anti-mouse NK1.1 (clone PK136)	BD Biosciences	624295
PE-Cyanine7 anti-mouse NK1.1 (clone PK136)	Thermo Fisher Scientific	25-5941-82; RRID:AB_469665
Brilliant Violet 785™ anti-mouse CD274 (B7-H1, PD-L1) (clone 10F.9G2)	Biolegend	124331; RRID:AB_2629659
PE-Cy5 anti-mouse TCR β Chain (clone H57-597)	BD Biosciences	553173; RRID:AB_394685
APC anti-mouse TNF-α (clone MP6-XT22)	Thermo Fisher Scientific	17-7321-82; RRID:AB_469508
BV650 anti-mouse TNF-α (clone MP6-XT22)	BD Biosciences	563943; RRID:AB_2738498
BV750 anti-mouse IFN-γ (clone XMG1.2)	BD Biosciences	566366; RRID:AB_2739713
PE anti-mouse IFN-γ (clone XMG1.2)	Thermo Fisher Scientific	12-7311-82; RRID:AB_466193
BV711 anti-mouse IL-10 (clone JES5-16E3)	BD Biosciences	564081; RRID: AB_2738581
PerCP-Cyanine5.5 anti-mouse IL-10 (clone JES5-16E3)	Thermo Fisher Scientific	45-7101-82; RRID: AB_996677
FITC anti-mouse IL-12 (clone C15.6)	BD Biosciences	560564; RRID:AB_1645243
PE anti-human/mouse Arginase 1 (Arg1)	R&D Systems	IC5868P; RRID:AB_10718118
APC anti-human/mouse Arginase 1 (Arg1)	R&D Systems	IC5868A; RRID:AB_2810265
BV650 anti-mouse CD19 (clone 1D3)	BD Biosciences	563235; RRID:AB_2738085
PE anti-human CD3 (clone UCHT1)	Thermo Fisher Scientific	12-0038-42; RRID:AB_10667884
PerCP/Cyanine5.5 anti-human CD4 (clone SK3)	Biolegend	980810
Brilliant Violet 421™ anti-human CD8a (clone RPA-T8)	Biolegend	301036; RRID:AB_10960142
FITC anti-human CD11b (clone MEM-174)	Thermo Fisher Scientific	MA1-19560; RRID:AB_1071193
APC/Cyanine7 anti-human CD11c (clone Bu15)	Biolegend	337218; RRID:AB_10662746

(*Continued on next page*)

Continued

REAGENT or RESOURCE	SOURCE	IDENTIFIER
PerCP-Cyanine5.5 anti-human CD33 (clone WM53)	Thermo Fisher Scientific	45-0338-42; RRID:AB_10714975
PE/Cyanine7 anti-human CD40 (clone 5C3)	Biolegend	334322; RRID:AB_10645472
Brilliant Violet 711™ anti-human CD45 (clone HI30)	Biolegend	304050; RRID:AB_2563466
APC anti-human CD68 (clone Y1/82A)	Biolegend	333810; RRID:AB_2275735
Brilliant Violet 605™ anti-human CD80 (clone 2D10)	Biolegend	305225; RRID:AB_11123909
FITC anti-human CD86 (clone BU63)	Thermo Fisher Scientific	MHCD8601; RRID:AB_10372961
Brilliant Violet 421™ anti-human HLA-DR (clone L243)	Biolegend	307636; RRID:AB_2561831
PE anti-human HLA-DR (clone TU36)	Thermo Fisher Scientific	MHLDR04; RRID:AB_10374185
PE anti-human Phospho-STAT3 (Tyr705) (clone LUVNKLA)	Thermo Fisher Scientific	12-9033-42; RRID:AB_2572679
anti-human/mouse CCRK antibody	Origene	AP13739PU-N
anti-human/mouse STAT3 antibody	Cell Signaling Technology	12640
anti-human/mouse Phospho-STAT3 (Tyr705) antibody	Cell Signaling Technology	9145
anti-human/mouse NFIL3 (E4BP4) antibody	Abcam	ab93785
anti-human/mouse HSP90 antibody	Cell Signaling Technology	4877
anti-human/mouse β-Tubulin antibody	Santa Cruz Biotechnology	sc-5274
anti-human/mouse Arginase 1 antibody	Thermo Fisher Scientific	PA5-85267
anti-human/mouse β-Actin antibody	Cell Signaling Technology	4970
Anti-mouse CD8a (clone 53-6.7)	Novus Biologicals	NBP1-49045
Anti-mouse CD8 alpha antibody	Abcam	ab217344
Anti-mouse CD11b antibody	Abcam	133357
Anti-mouse Ly6C antibody	CiteAb	ab15627
Anti-mouse Ly6G antibody	CiteAb	127602
Goat anti-Rabbit IgG (H+L) Secondary Antibody, HRP	Thermo Fisher Scientific	31460; RRID:AB_228341
Goat anti-Mouse IgG (H+L) Secondary Antibody, HRP	Thermo Fisher Scientific	31430; RRID:AB_228307
Goat anti-Rabbit IgG (H+L) Cross-Adsorbed Secondary Antibody, Alexa Fluor™ 488	Thermo Fisher Scientific	A-11008; RRID:AB_143165
Donkey anti-Rabbit IgG (H+L) Highly Cross-Adsorbed Secondary Antibody, Alexa Fluor™ 555	Thermo Fisher Scientific	A-31572; RRID:AB_162543
Goat anti-Rat IgG (H+L) Cross-Adsorbed Secondary Antibody, Alexa Fluor™ 488	Thermo Fisher Scientific	A-11006; RRID:AB_2534074
Bacterial and virus strains		
Vpx-containing HIV-1-based lentiviral vector	Gift from Prof. Nathaniel R.	
Lentiviral shRNA vectors targeting mouse Ccrk (shCcrk)	Adopted from our previous publication	
Biological samples		
Blood, tumor and adjacent non-tumor liver tissues from patients with HCC and healthy donors	Prince of Wales Hospital (Hong Kong)	N/A
Chemicals, peptides, and recombinant proteins		
Puromycin dihydrochloride	Santa Cruz Biotechnology	sc-108071
pcDNA™3.1 (+) Mammalian Expression Vector	Invitrogen	V79020
FuGENE HD transfection reagent	Roche	04709691001
Ficoll-Paque Premium	GE Healthcare	17-5442-03
gentleMACS Dissociators	Miltenyi Biotec	130-093-235
anti-CD3 microbeads	Miltenyi Biotec	130-050-101

(*Continued on next page*)

Continued

REAGENT or RESOURCE	SOURCE	IDENTIFIER
anti-CD33 microbeads	Miltenyi Biotec	130-045-501
anti-Ly6G microbeads	Miltenyi Biotec	130-120-337
Carboxyfluorescein succinimidyl ester (CFSE)	Invitrogen	C2210
TRIzol	Invitrogen	15596026
Cocktail	Roche	11697498001
Magna ChIP™ Protein A+G Magnetic Beads	Millipore	16-663
Recombinant Human IL-2 Protein	R&D system	202-IL
Fixation and Permeabilization Solution	BD Biosciences	554722
T-PER Tissue Protein Extraction Reagent	Thermo Fisher Scientific	78510
TB Green® Premix Ex Taq™ II	Takara	RR820A
WesternBright® Sirius® Luminol/enhancer solution	Advansta	R-03027
WesternBright® Peroxide Chemiluminescent Detection Reagent	Advansta	R-03025
CrystalMount® Mounting Medium	Histovabio	CMT105
Heparin sodium salt	Sigma-Aldrich	H4784
Fetal Bovine Serum	Gibco	10500064
PBS tablets	Gibco	18912014
Critical commercial assays		
Neon™ Transfection System	Thermo Fisher Scientific	MPK5000
PrimeScript™ RT Reagent Kit (Perfect Real Time)	Takara	RR037A
Pierce™ BCA Protein Assay Kit	Thermo Fisher Scientific	23225
QIAquick PCR Purification Kit	Qiagen	28104
mMESSAGE mMACHINE™ T7 Transcription Kit	Thermo Fisher Scientific	AM1344
MEGAclear™ Transcription Clean-Up Kit	Thermo Fisher Scientific	AM1908
Human IFN-γ ELISA kit	Invitrogen	88-7316-22
Experimental models: Cell lines		
C57BL/6-derived Hepatoma Cell Line RIL-175	Gift from Prof. Lars Zender and Prof. Tim F. Greten	
Human myeloid cell line U-937	ATCC	CRL-1593.2
293T cells	ATCC	CRL-3216
Oligonucleotides		
qPCR primers	This paper	See in Table S1
ChIP-qPCR primers	This paper	See in Table S1
Software and algorithms		
GraphPad Prism 8	GraphPad Software, Inc	https://www.graphpad.com
FACSDIVA Software	BD Biosciences	https://www.bdbiosciences.com
FlowJo 10.8.1	Tree Star	https://www.flowjo.com
ImageJ	NIH	https://imagej.nih.gov/ij/

RESOURCE AVAILABILITY

Lead contact

Further information and requests for resources and reagents should be directed to and will be fulfilled by the Lead Contact, Alfred Sze-Lok Cheng (alfredcheng@cuhk.edu.hk).

Materials availability

All unique/stable reagents generated in this study are available from the lead contact with a completed Materials Transfer Agreement.

Data and code availability

- This paper does not analyze existing, publicly available data.
- All data reported in this paper will be shared by the lead contact upon request.
- This paper does not report original code.
- Any additional information required to reanalyze the data reported in this paper is available from the lead contact upon request.

EXPERIMENTAL MODEL AND STUDY PARTICIPANT DETAILS

Patient specimens

Paired blood, tumor and adjacent non-tumor liver tissues from 14 patients with HCC who underwent liver resection at the Prince of Wales Hospital (Hong Kong) were collected for myeloid cell sorting and quantitative reverse transcription-PCR (qRT-PCR) analysis. Buffy coats of healthy subjects from Red Cross Blood (Hong Kong) were also included as controls. Studies using human specimens were approved by the joint CUHK-NTEC Clinical Research Ethics Committee.

Cell lines

Cells were incubated at 37°C in a humidified chamber containing 5% CO_2. Mouse hepatoma RIL-175 cell line was provided by Prof. Tim F. Greten (National Cancer Institute, National Institutes of Health, Bethesda, USA) and Prof. Lars Zender (University Hospital Tubingen, Germany)[27] and maintained in high-glucose DMEM (Gibco; Invitrogen) supplemented with 10% FBS (Hyclone). *Ccrk*-knockdown RIL-175 cells were generated by transduced with a lentivirus expressing sh*Ccrk* and selected as previously described.[26] Single clone was sorted by FACSArial Fusion (BD Biosciences) and *Ccrk* knockdown was confirmed by qRT-PCR and western blot. Human myeloid cell line U937 was purchased from the American Type Culture Collection and maintained in RPMI1640 (Gibco; Invitrogen) supplemented with 10% FBS (Hyclone). *CCRK*-expressing or control vector pcDNA3.1 (Invitrogen) were transfected into CCRK low-expressed U937 cells using FuGENE HD transfection reagent (Roche) and selected by puromycin to establish stable cell lines as previously.[4] *E4BP4* knockdown was conducted by transduced U937-CCRK cells with a lentivirus expressing sh*E4BP4* (GenePharma), and a control sh*Ctrl* stable cell line was constructed in parallel, followed by puromycin selection. CCRK and E4BP4 expressions were confirmed by qRT-PCR and western blot.

Mice

Six to eight-week-old male C57BL/6 and B6.Cg-Tg(CAG-DsRed*MST)1NaFgy/J mice were obtained and housed at Laboratory Animal Services Centre (LASEC) of the Chinese University of Hong Kong (CUHK). $Ccrk^{indel/indel}$ transgenic (TG) mouse was generated in Hong Kong University of Science and Technology (HKUST) and then imported into CUHK for further *in vivo* experiments. All animal experiments were carried out in accordance with the guidelines approved by the Animal Experimentation Ethics Committee (AEEC) of CUHK and Animal Ethic Committee (VPRDO) of HKUST.

METHOD DETAILS

Single cell isolation and flow cytometry analysis

Peripherial blood mononuclear cells (PBMCs) were freshly isolated from buffy coats of anonymous human healthy donors using Ficoll-Paque Premium (GE Healthcare). Single cells were isolated from fresh liver and tumour tissues by gentleMACS Dissociators (Miltenyi Biotec) following manufacturer's instructions. Cells were collected and washed, and counted as numbers per gram of tissue. $5*10^6$ single cells/tube were be collected and blocked with Mouse BD Fc Block (BD Biosciences) and True Stain Monocyte Blocker (BioLegend). For surface staining, the antibody mix was prepared with Brilliant Stain Buffer Plus (BD Biosciences) and incubated with the samples for 20 min at 4°C. For intracellular markers, the cells were subsequently permeablised with Transcription Factor Buffer Set (BD Biosciences) according to the manufacture's protocol. Samples were stained with intracellular antibodies for 50 min at 4°C and washed by Perm wash buffer (BD Biosciences). Flow cytometry was performed using BD FACSAria Fusion or BD FACSymphony A5 Cell Analyzer (BD Biosciences). Spectral unmixing and high-parameter analysis was performed by FlowJo v10 Software using the UMAP, FlowSOM and ClusterExplorer plugins (BD Biosciences). The cell proportions and absolute number would be calculated. The antibodies used are listed in the key resources table.

Quantitative RT-PCR

Total RNA was extracted by using TRIzol reagent (Invitrogen). 1 μg RNA was reverse transcribed to cDNA using Reverse Transcription Master Kit (Takara) according to the manufacturer's instructions. For quantitative PCR analysis, aliquots of cDNA were amplified using TB Green Premix Ex Taq II (Takara) and ViiATM7/QuantStudio 7 Flex Real Time PCR System (Applied Biosystems). GAPDH was used as an internal control. All reactions were performed in triplicate. The sequences of primers used are listed in the key resources table.

Western blot

Protein lysates from primary cells or cell lines were prepared using protease inhibitor cocktail-containing (Roche) lysis buffer (50 mM Tris-HCl, pH 7.5, 150 mM NaCl, 1% NP-40, 0.5% Na-deoxycholate) and T-PER Tissue Protein Extraction Reagent (Thermo Scientific), respectively. Protein concentration was determined by the Pierce™ BCA Protein Assay Kit (Thermo Fisher Scientific). 40-80 μg of protein was resolved by 10%

SDS-polyacrylamide gel electrophoresis and electroblotted onto equilibrated nitrocellulose membrane (Bio-Rad Laboratories). Membranes were incubated with primary antibodies at 4°C overnight followed by secondary antibodies for 2 h at room temperature. Antibody-antigen complexes were detected using the WesternBright Sirius Luminol/enhancer solution and WesternBright Peroxide Chemiluminescent Detection Reagent (Advansta). The antibodies used are listed in the key resources table.

Mouse BM-derived MDSCs

Bone marrow (BM) was harvested from naïve B6.Cg-Tg(CAG-DsRed*MST)1NaFgy/J ($RFP^{+/+}$) C57BL/6 mice and plated at 2×10^6 cells/mL in Dulbecco modified Eagle medium plus 10% fetal calf serum, 10 mM N-2-hydroxyethylpiperazine-N′-2-ethanesulfonic acid buffer, 1 mM sodium pyruvate, 100 U/mL penicillin, 100 mg/mL streptomycin, and 2 mM L-glutamine, 40 ng/mL granulocyte macrophage colony-stimulating factor (GM-CSF) and IL-6 at 37°C at 10% CO_2 for 4 days.

Lentivirus preparation and infection

Lentivirus constructed for efficient transduction of myeloid cells was prepared using a protocol as previously described.[28] The plasmids of lentiviral backbone were kindly provided by Prof. Nathaniel R. Landau, including pRSV-Rev, pVSV-G, pMDL and PcVpx.myc. Briefly, $5*10^6$ 293T cells in a 10 cm dish were co-transfected by the calcium phosphate method with 14 μg pLenti-CMV-eGFP-sh*Ctrl* or -sh*Ccrk* (Dharmacon),[26] 2.5 μg pRSV-Rev, 3.5 μg pVSV-G, 1.7 μg PcVpx.myc and 5 μg pMDL. The viral supernatants were harvested 48 h post-transfection, passed through a 0.45 μm pore-size filter. Lentivirus particles were enriched by ultracentrifuge 120 min at 40,000 × g, 4°C and resuspend in PBS, aliquoted and stored at -80°C. Virus titer was determined as transducing unites (TU/mL) as previously described.[26,28] 1 multiplicity of infection (MOI) was used to infect BM-MDSCs as optimized dose. The number of infected cells indicated by GFP positive cells was quantified and enriched by FACSAria Fusion (BD Biosciences) according to the manufacturer's protocols.

Generation of *Ccrk*$^{indel/indel}$ transgenic (TG) mouse

Ccrk$^{indel/indel}$ transgenic (TG) mouse line bearing a ATC (encodes amino acid Ile) insertion in *Ccrk* exon 3 between c.219 and c.220 was generated by injection of the CRISPR-Cas9 mRNA and *Ccrk* sgRNA into the zygotes of C57BL/6 mouse. The CRISPR-Cas9 mRNA was prepared by amplification of the Cas9 coding sequence with addition of T7 promoter sequence and generated by mMESSAGE mMACHINE T7 kit. The guide sequence for *Ccrk* exon 3 was cloned into the sgRNA expression vector, amplified by 5′-TTAATACGACTCACTATAGGAGCA CAAAGCCCGCACCATG-3′ and 5′-AAAAGCACCGACTCGGTGCC-3′ from sgRNA expression vector with addition of T7 promoter sequence, and generated by MEGAshortscript T7 transcription kit. The CRISPR- Cas9 mRNA and *Ccrk* sgRNA were purified by MEGAclear kit before injection. The injection process was done by Animal & Plant Care Facility (APCF) in the HKUST and approved by Animal Ethic Committee (VPRDO). A heterozygous insertion mutation *Ccrk*$^{indel/-}$mouse was identified by DNA sequencing to confirm the insertion of Ile (ATC) between His73 and Gly74. Homozygous *Ccrk*$^{indel/indel}$ was generated by cross-breeding of heterozygous mouse and confirmed by DNA sequencing. More than 10 rounds of backcrossing with C57BL/6 were performed to fix the *Ccrk* insertion mutation and to clean up the genetic background. The sequences of primers for genotyping are listed in key resources table.

In vivo experiments

For *in vivo* BM-MDSC differentiation experiment, BM-MDSCs were generated from BM of B6.Cg-Tg(CAG-DsRed*MST)1NaFgy/J ($RFP^{+/+}$) C57BL/6 mice and infected by lentivirus-sh*Ctrl* or -sh*Ccrk*. GFP^+RFP^+MDSCs were sorted by FACS at 48h post infection. 2×10^6 purified GFP^+RFP^+MDSCs cells were injected into naïve C57BL/6 mice via tail vein. Mice were then sacrificed at 24h post MDSC adoptive transfer and blood samples were collected. Mouse PBMCs were isolated as previously described and stained with anti-mouse CD11b, GR-1, Ly6G, Ly6C, F4/80, CD11c, CD80, and CD86 antibodies. The data were acquired by flow cytometry using FACS Fortessa/FACSAria Fusion (BD Biosciences) and analyzed by FlowJo software (Tree Star).

To study the effect of BM-MDSC in subcutaneous tumor growth, lentivirus-sh*Ctrl* or -sh*Ccrk*-treated GFP^+RFP^+MDSCs were purified as described above. 2×10^6 purified GFP^+RFP^+MDSC-sh*Ctrl* or -sh*Ccrk* were then injected intratumorally into the left or right subcutaneous tumors of the same C57BL/6 receipt mouse after RIL-175 subcutaneous tumor inoculation at day 6. Subcutaneous tumor growth was measured every other day by external caliper. The tumor size was obtained using the formula (W(2) × L)/2 (W, width; L, length). Mice were sacrificed at day 14 post tumor inoculation and $CD8^+$T cell number was determined by flow cytometry.

For the orthotopic HCC model, $5x10^5$ RIL-175 cells were injected into the liver of wild type (WT) C57BL/6 or *Ccrk*$^{indel/indel}$ TG mice. Mouse body weight was monitored every other day and mouse survival were documented, and then sacrificed at 3 weeks post-tumor cell inoculation or at endpoints approved by CUHK-AEEC. Tumor, liver, spleen and blood were collected for primary cell isolation and high-dimensional flow cytometry analysis BD FACSymphony A5 Cell Analyzer (BD Biosciences). The antibodies used for flow cytometry analysis are listed in key resources table.

Human MDSC proliferation and differentiation assays

PBMCs isolated from healthy donors were plated at 1×10^6 cells/mL in RPMI1640 plus 10% fetal calf serum, 10 mM N-2-hydroxyethylpiperazine-N′-2-ethanesulfonic acid buffer, 1 mM sodium pyruvate, 100 U/mL penicillin, 100 mg/mL streptomycin, and 2 mM L-glutamine, 10 ng/mL GM-CSF and IL-6 at 37°C at 10% CO_2 for 7 days with half medium refresh every other day. $CD33^+$MDSCs were then enriched by anti-CD33

mcirobeads (Miltenyi Biotec). 100 nM siRNAs against CCRK (si*CCRK*: 5′-GGCGGUUGGAGGACGGCUU-3′), and a control sequence (si*Ctrl*: 5′-UUCUCCGAACGUGUCACGU-3′)[4] were transfected into the purified $CD33^+$MDSCs by Neon™ Transfection System (ThermoFisher) according to the manufacturer's protocols. Cells were collected 24-hour post-transfection for RNA extraction and 48 h post-transfection for protein isolation. For MDSC proliferation assay, carboxyfluorescein succinimidyl ester (CFSE; 5 μmol/L; Invitrogen) was used to label purified $CD33^+$MDSCs before siRNA treatment. Cells were collected at 72-hour post-transfection and CFSE signals were acquired by flow cytometry using FACSAria Fusion (BD Biosciences). For phenotype analysis, $CD33^+$MDSCs treated with si*Ctrl* or si*CCRK* were collected at 48-hour post-transfection, and analysed by flow cytometry using FACSAria Fusion (BD Biosciences). The antibodies used are listed in the key resources table.

Mixed lymphocyte reaction (MLR) assay

$CD33^+$MDSCs treated with si*Ctrl* or si*CCRK* were collected at 48-hour post-transfection. Allogenic $CD3^+$T cells were purified by anti-human CD3 microbeads and labelled with CFSE(5 μmol/L; Invitrogen) and co-cultured with siRNA-treated $CD33^+$MDSCs (1:1) in the presence of human recombinant IL-2 (R&D) for 3 days. T cells cultured alone was used as negative control. Supernatant was collected for IFN-γ detection by ELISA (Invitrogen) according to the manufacturer's protocols. Cells were collected and CFSE signals on T cells were acquired by flow cytometry using FACSAria Fusion (BD Biosciences). The antibodies used are listed in the key resources table.

Chromatin immunoprecipitation-quantitative PCR (ChIP-qPCR)

U937-vector or -CCRK stable cell lines were collected directly crosslinked with 1% formaldehyde in the culture plate and the reaction was stopped by glycine. Fixed cells were collected and lysed with SDS-Lysis buffer containing proteinase inhibitor. The lysates were fragmented into 200-300 bp by Bioruptor (Diagenode, Denville, New Jersey, USA). ChIP-graded rabbit anti- STAT3 or E4BP4 antibodies were conjugated with magnetic beads (Magna ChIP™ Protein A+G Magnetic Beads) by rotation in cold room (4°C) for 1 hour. Meanwhile, the cell lysates were incubated with magnetic beads and rotated in cold room (4°C) for 1 hour, to remove endogenous antibodies. Cell lysates were then incubated with magnetic beads-conjugated antibodies and rotated in cold room (4°C) for 12-16 hours. After washing and reversed crosslinking, the immunoprecipitated DNA was purified by purification kit (Qiagen), followed by ChIP-qPCR with gene region-specific primer pairs. The sequences of primers used are listed in the key resources table.

Immunofluorescence staining

Mouse tumor tissues were collected and fixed in 4% paraformaldehyde (Sigma-Aldrich) for 24 hours, then washed in 70% ethanol and embedded in paraffin. After dewaxing and antigen-retrieving, five-millimeter sections from embedded tumors were incubated with primary antibodies at 4°C overnight, followed by secondary antibodies for 1.5-hour at room temperature. Finally, the slides were counterstained with DAPI for nucleus for 5-10 min and mounted with CrystalMount® Mounting Medium. The immunofluorescence signals were detected by Axioscan 7 Automatic Slide Scanner (Zeiss, Germany). The antibodies used for immunofluorescence staining are listed in key resources table.

QUANTIFICATION AND STATISTICAL ANALYSIS

At least 5 mice were included in each group, unless noted and the experiments were repeated a minimum 2 times. GraphPad Prism 8 software was used for statistical analysis. The difference between groups was evaluated by Mann-Whitney U test, unpaired Student's t-test, or one-way analysis of variance (ANOVA) with Dunnett's multiple comparisons correction. The normality of data was confirmed by Shapiro-Wilk test with a P value greater than 0.05 when unpaired Student's t-test was applied. Correlation was calculated as Pearson's correlation coefficient. Kaplan-Meier survival analysis with log-rank Mantel-Cox test was used to compare differences in overall survival between groups of mice. Data are presented as mean ± SD. A P value smaller than 0.05 was considered statistically significant.